[47] S.M. Zou, P. Erbacher, J.S. Remy, J.P. Behr, Systemic linear polyethylenimine (L-PEI)-mediated gene delivery in the mouse, J. Gene Med. 2 (2) (2000) 128–134.
[48] I. Chemin, D. Morsdour, S. Wieland, W.B. Offensperger, E. Walter, J.P. Behr, H.E. Blum, Liver-directed gene transfer: a linear polyethlenimine derivative mediates highly efficient DNA delivery to primary hepatocytes *in vitro* and *in vivo*, J. Viral Hepat. 5 (6) (1998) 369–375.
[49] V.A. Polunovsky, C.H. Wendt, D.H. Ingbar, M.S. Peterson, P.B. Bitterman, Induction of endothelial cell apoptosis by TNF alpha: modulation by inhibitors of protein synthesis, Exp. Cell Res. 214 (2) (1994) 584–594.
[50] L.F. Fajardo, H.H. Kwan, J. Kowalski, S.D. Prionas, A.C. Allison, Dual role of tumor necrosis factor-alpha in angiogenesis, Am. J. Pathol. 140 (3) (1992) 539–544.
[51] N. Watanabe, Y. Niitsu, H. Umeno, H. Kuriyama, H. Neda, N. Yamauchi, M. Maeda, I. Urushizaki, Toxic effect of tumor necrosis factor on tumor vasculature in mice, Cancer Res. 48 (8) (1988) 2179–2183.
[52] P.L. Naredi, P.G. Linder, S.B. Holmberg, U. Stenram, A. Peterson, L.R. Hafstrom, The effects of tumour necrosis factor alpha on the vascular bed and blood flow in an experimental rat hepatoma, Int. J. Cancer 54 (4) (1993) 645–649.
[53] S. Loisel, C.L. Gall, L. Doucet, C. Ferec, V. Flock, Contribution on plasmid DNA to hepatotoxicity after systemic administration of polyplexes, Hum. Gene Ther. 12 (6) (2001) 685–696.
[54] K. Aoki, S. Furuhata, K. Hatanaka, M. Maeda, J.S. Remy, J.-P. Behr, M. Terada, T. Yoshida, Polyethyleneimine-mediated gene transfer into pancreatic tumor dissemination in the murine peritoneal cavity, Gene Ther. 8 (7) (2001) 508–514.
[55] M. Blick, S.A. Sheriwin, M. Rosenblum, J. Gutterman, Phase I study of recombinant tumor necrosis factor in cancer patients, Cancer Res. 47 (11) (1987) 2986–2989.
[56] P.J. Creaven, J.E. Plager, S. Dupere, R.P. Huben, H. Takita, A. Mittelman, A. Proefrock, Phase I clinical trial of recombinant human tumor necrosis factor, Cancer Chemother. Pharmacol. 20 (2) (1987) 137–144.
[57] T. Moritz, N. Niederle, J. Baumann, D. May, E. Kurschel, R. Osieka, J. Kempeni, E. Svhlick, C.G. Schmidt, Phase I study of recombinant human tumor necrosis factor alpha in advanced malignant disease, Cancer Immunol. Immunother. 29 (2) (1989) 144–150.
[58] W.L. Furman, D. Strother, K. McClain, B. Bell, B. Leventhal, C.B. Pratt, Phase I clinical trial of recombinant human tumor necrosis factor in children with refractory solid tumors: a pediatric oncology group study, J. Clin. Oncol. 11 (11) (1993) 2205–2210.
[59] S.A. Rosenberg, Gene therapy for cancer, J. Am. Med. Assoc. 268 (17) (1992) 2416–2419.
[60] S. Moriuchi, T. Oligino, D. Krisky, P. Marconi, D. Fink, J. Cohen, J.C. Glorioso, Enhanced tumor cell killing in the presence of ganciclovir by herpes simplex virus type 1 vector-directed coexpression of human tumor necrosis factor-α and herpes simplex virus thymidine kinase, Cancer Res. 58 (24) (1998) 5731–5737.
[61] B. Yamini, X. Yu, P. Pytel, N. Galanopoulos, V. Rawlani, J. Veerapong, K. Bickenbach, R.R. Weichselbaum, Adenovirally delivered tumor necrosis factor-α improves the antiglioma efficacy of concomitant radiation and temozolomide therapy, Clin. Cancer Res. 13 (20) (2007) 6217–6223.

DOI: 10.1002/anie.201203360

siRNA Delivery

A Phenylboronate-Functionalized Polyion Complex Micelle for ATP-Triggered Release of siRNA**

*Mitsuru Naito, Takehiko Ishii, Akira Matsumoto, Kanjiro Miyata, Yuji Miyahara, and Kazunori Kataoka**

Therapeutics based on small interfering RNA (siRNA) offer an attractive clinical option because of its ability to silence genes in a highly sequence-specific manner. [1] A key challenge lies in developing a delivery system that helps protect the siRNAs from endogenous RNase degradation while allowing for controlled pharmacokinetics. One promising approach is a formulation of polyion complex (PIC) micelles that spontaneously form in an aqueous environment simply through electrostatic interactions between the anionic siRNA and cationic polymers.[2] With versatile designs of the counterpart cationic polymers, representative poly(ethylene glycol) based block co-polymers, many creative PIC-based strategies have emerged, some of which have shown encouraging in vitro gene silencing abilities.[3–5] However, in general, these PIC-based carriers suffer from instability under physiological conditions, primarily because of the relatively short chain length of the siRNA, that is 20–25 nucleotides, which results in poor thermodynamic stability. Therefore, stabilization of the PIC-based carriers so that programmed destabilization upon arrival at the site of intracellular targets (to release siRNA) has been of interest. Current efforts have focused on either one or combinations of the following three representative approaches: covalent conjugation of siRNAs to a homing polymer,[3,6–8] introduction of hydrophobic moieties to reinforce the core-aggregation,[9–11] and cross-linking the core aggregate by disulfide bridging.[5,12] As such, the combination of these approaches often results in a highly complex structure and method of preparation.

Herein, we describe a sophisticated solution that can remarkably simplify the synthesis of PICs. It uses a phenylboronate functionality, which incorporates all of the aforementioned methods of stabilization (Scheme 1) while maintaining a wide window of control for environmental sensitivity. Phenylboronic acid (PBA) is a synthetic molecule capable of forming reversible covalent esters with 1,2- or 1,3-*cis*-diols including on a ribose ring,[13–15] a structure which is present at the 3′ end of RNAs and several kinds of ribonucleotides. Because of this property, PBA has historically been used as a ligand for RNA in affinity chromatography.[16] Therefore, this binding property offers a facile route for chemical conjugation of siRNAs to the pendant PBA groups. Once electrostatically condensed into the PIC, the chances of equilibrium binding are increased, in which intermolecular cross-links could also form because of the bis-bidentate ribose arrangement at the 3′ end of the double-stranded siRNA, thereby further stabilizing the complex. Furthermore, PBA is unique in that it undergoes a dramatic inversion in its level of hydrophobicity depending on the degree of acid disassociation;[17] it is strongly hydrophobic when uncharged but it becomes hydrophilic when negatively charged at pH values above its pK_a. As shown in Figure 1, the binding between PBA and siRNAs is essentially a reversible equilibrium process dependent on the concentrations of each species. These features can be used to fine-tune or switch the stability of the complex, which is relevant to creating a system that is sensitive to the inter- and intracellular environments. Herein, we demonstrate that the PBA-assisted PIC micelles can be tailored to exhibit a dramatic disruption accompanied by the release of siRNAs in response to a change in the ribose concentration (which parallels events in the intracellular environment).

A platform cationic polymer poly(ethylene glycol)-*block*-poly(L-lysine) (PEG-*b*-PLys) was first prepared, the lysine residues of which were quantitatively modified with 3-fluoro-4-carboxyphenylboronic acid (FPBA) to different extents. The weight-average molecular weight (M_w) of PEG and the mean degree of polymerization of PLys were determined to be 12000 Da and 42, respectively (Supporting Information, Table S1). The synthesized polymers are referred to as PEG-*b*-P(Lys/FPBA$_X$)$_{42}$, where X denotes number of FPBA units introduced per polymer chain. According to the scattered light intensity of the polymer solutions, polymers were soluble (at 5 mg mL^{-1}) in HEPES buffered solution (HBS, pH 7.3) up to 55% FPBA modification, that is (PEG-*b*-P(Lys/FPBA$_{23}$)$_{42}$, however, those with 66% (that is (PEG-*b*-P(Lys/FPBA$_{28}$)$_{42}$) or higher degrees of FPBA modification were partially insoluble because of the strong hydrophobicity of FPBA (data not shown). The HBS-soluble series of polymers, that is PEG-*b*-P(Lys/FPBA$_{0,10,19,23}$)$_{42}$, were allowed to complex with siRNA at various N/P ratios, which is defined as the molar

[*] M. Naito, Dr. K. Kataoka
Department of Materials Engineering, The University of Tokyo
Hongo 7-3-1, Bunkyo-ku, Tokyo 113-8656 (Japan)
E-mail: kataoka@bmw.t.u-tokyo.ac.jp
Homepage: http://www.bmw.t.u-tokyo.ac.jp/
Dr. T. Ishii
Department of Bioengineering, The University of Tokyo (Japan)
Dr. A. Matsumoto, Dr. Y. Miyahara
Institute of Biomaterials and Bioengineering, Tokyo Medical and Dental University (Japan)
Dr. K. Miyata
Division of Clinical Biotechnology, Center for Disease Biology and Integrative Medicine, The University of Tokyo (Japan)

[**] This research is supported by the Japan Society for the Promotion of Science (JSPS) through the "Funding Program for World-Leading Innovative R&D on Science and Technology (FIRST Program)."

Supporting information for this article is available on the WWW under http://dx.doi.org/10.1002/anie.201203360.

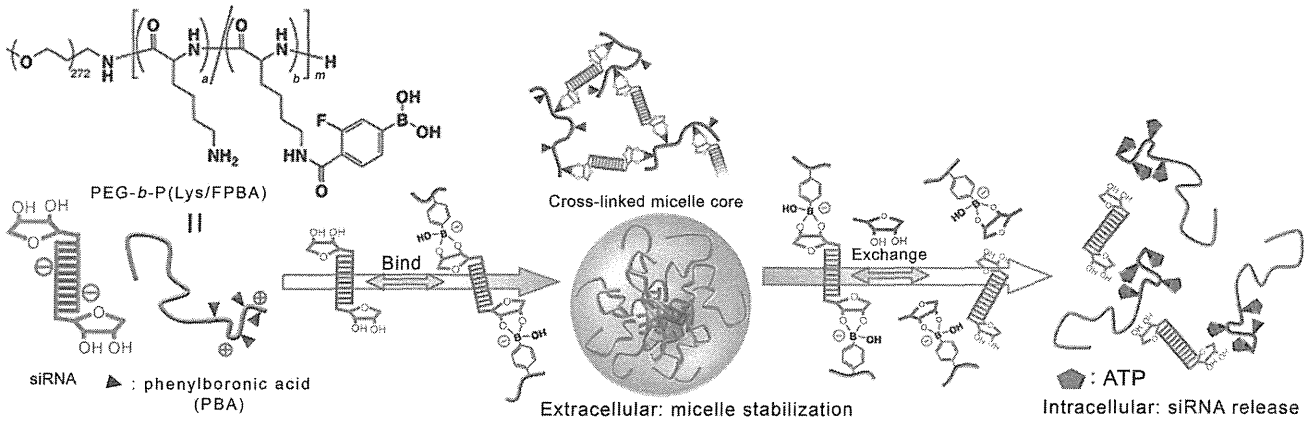

Scheme 1. Schematic representation of the phenylboronic acid based strategy for siRNA delivery; the chemical formula of the polymer, enhanced stability of the micelle, and the mechanism of selective intracellular release are shown.

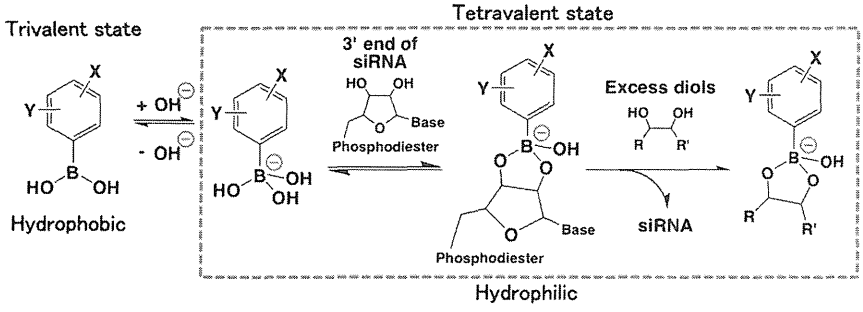

Figure 1. Equilibrium between a PBA derivative binding to siRNAs and other diols in aqueous solution.

ratio of the primary amino groups in the PLys segments to the phosphate groups in the siRNAs. These polymers were assessed by fluorescence correlation spectroscopy (FCS) with regard to the stability of the complex (Figure 2a). From measured values of the diffusion coefficient (D) relative to that for the free siRNA (72.0 $\mu m^2 s^{-1}$), we concluded that PEG-*b*-PLys$_{42}$ with no FPBA modification and PEG-*b*-P(Lys/FPBA$_{10}$)$_{42}$ (the lowest FPBA content of the series) could not form complexes with siRNAs under physiological salt condition in the presence of 10% fetal bovine serum (FBS), although the latter was found to form a complex in the absence of FBS (see Figure S1). In contrast, complexes of PEG-*b*-P(Lys/FPBA$_{19}$)$_{42}$ and PEG-*b*-P(Lys/FPBA$_{23}$)$_{42}$, with increased FPBA content, do tolerate such conditions. Indeed, PEG-*b*-P(Lys/FPBA$_{23}$)$_{42}$, with the highest FPBA content of the series, showed no significant change in its diffusion coefficient regardless of the presence of FBS (Figure 2a, see also Figure S1c). PEG-*b*-P(Lys/FPBA$_{19}$)$_{42}$ and PEG-*b*-P(Lys/FPBA$_{23}$)$_{42}$ were further compared by agarose gel electrophoresis at a fixed N/P ratio of 4 (above which no more change in the diffusion coefficient was observed in Figure 2a) in the presence of a complex-destabilizer polyanionic dextran sodium sulfate (DSS, $M_w = 5000$ Da; Figure 2b). In this experiment, bands of Cy3-labeled siRNA, which are indicative of partial or whole collapse of the complex, could be seen at the bottom of each lane. In both cases, the bands became more intense with increasing concentrations of DSS (or increasing A/P ratio in Figure 2b), which destabilizes the complex because its polyanionic charges replace the PIC-engaged siRNAs. Even so, in comparison, the complex of PEG-*b*-P(Lys/FPBA$_{23}$)$_{42}$ shows relatively high resistance to DSS. Thus, these results establish that the stability of the complex has been increased by the PBA functionality, presumably because of its multiple modes of stabilization, as described above.

To gain more clear insight into the siRNA release, three distinct types of double-stranded siRNAs were prepared (Figure 3), that is a normal one terminated with ribose at both 3′ ends (R-siRNA-R) and those modified with deoxyribose at either one (R-siRNA-dR) or both 3′ ends (dR-siRNA-dR), so that each represents bi-, mono-, or non-functionality when binding with PBA (Figure 3). Each siRNA was complexed with PEG-*b*-P(Lys/FPBA$_{23}$)$_{42}$, with various N/P ratios, and analyzed by gel electrophoresis (Figure 3). In this experiment, bands in the gel can be attributed to free siRNA that did not participate in complex formation under each condition. Therefore, the intensity of the bands decreases with an increasing N/P ratio for all cases, which is consistent with Figure 2a. By comparing the three systems, it can be observed that the trend is in accord with the number of the ribose functionalities, R-siRNA-R > R-siRNA-dR > dR-siRNA-dR, indicating the order of binding efficiency. Accordingly, this result supports an important role for the PBA–siRNA binding in the stabilization of the complex.

Further evidence for ribose-specific stabilization and its sensitivity to the surrounding environment was determined by analysis of complexes subjected to competitive ribose or non-ribose environments. For competitors, adenosine triphosphate (ATP), uridine monophosphate (UMP), deoxythymidine monophosphate (dTMP), and glucose were each assessed at their in vivo concentrations. Note that among

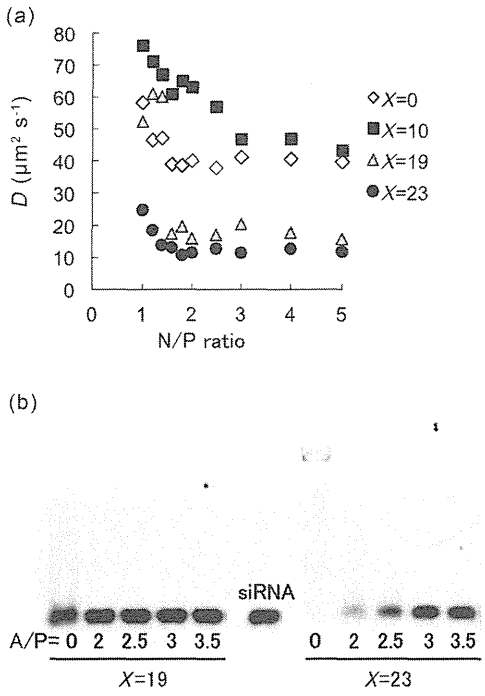

Figure 2. Stability of the complex between R-siRNA-R and PEG-*b*-P(Lys/FPBA$_X$)$_{42}$. a) Diffusion coefficients of Cy3-labeled siRNA in various polymer-complexes as a function of N/P ratio, as determined by FCS, after a 1 h incubation in HBS containing 10% FBS. b) Agarose gel electrophoresis of the complex for $X=19$ (left) and $X=23$ (right) at N/P=4 after a 1 h incubation in HBS containing DSS. A/P denotes the molar ratio of the anionic charges in DSS to the phosphate groups in the siRNA.

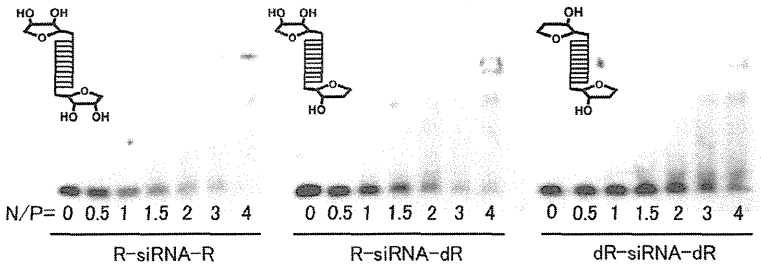

Figure 3. Agarose gel electrophoresis of the complex formed between PEG-*b*-P(Lys/FPBA$_{23}$)$_{42}$ and different types of double-stranded siRNAs; R-siRNA-R (left), R-siRNA-dR (middle) and dR-siRNA-dR (right), for various N/P ratios, after a 4 h incubation in HBS.

these additives only ATP and UMP have ribose moieties, which have the potential to compete with siRNA for binding to PBA. Figure 4a shows changes in the diffusion coefficient of the siRNA (R-siRNA-R) complexed with PEG-*b*-P(Lys/FPBA$_{23}$)$_{42}$ as a function of the concentration of the additive. As expected, the complex is markedly destabilized, as seen by increasing diffusion coefficients, upon addition of ATP and UMP. On the contrary, neither dTMP, incapable of binding to PBA, nor glucose, the most abundant polyol in the blood (normally approximately 10 mM) with relatively weak binding affinity to PBA, caused any significant destabilization even when high concentrations were used. Interestingly, the complex is more sensitive to the triphosphate ATP than it is to a monophosphate UMP. This difference may be due to the different number of the phosphate anions of each molecule. That is to say, the higher anionic density of ATP, upon binding with the pendant PBA, should aid in both electrostatic repulsion against the siRNA and also weaken the core hydrophobic interaction of PBA more than UMP. Figure 4b compares the stability of complexes consisting of di-, mono- and non-ribose functionalized siRNAs when exposed to ATP. In accordance with Figure 3, the complex stability (that is resistance to ATP) strikingly depends on the number of ribose functionalities. Such graded control of the complex stability, depending on the type of siRNA, should be of benefit to fine-tuning the release of siRNAs. Significantly lower, but still appreciable ATP resistance, was shown by the dR-siRNA-dR complex; this confirmed that the contribution of the hydrophobic PBA interaction was significant to the resultant stability. However, as illustrated in Figure 1, the fraction of trivalent hydrophobic PBA, which is responsible for such a hydrophobic interaction, can dramatically decrease with increased ribose concentration. Also the most abundant ribonucleotide in vivo, ATP, is present in the extracellular environment at about 0.4 mM, but is dramatically higher (up to 3 mM) within the intracellular matrix.[18–20] Results shown in Figure 4 demonstrate that the PIC will respond to ATP concentrations of exactly this range, thus offering the potential for the selective release of siRNAs upon entry into the cell. Preliminary studies of the R-siRNA-R engaged complex of PEG-*b*-P(Lys/FPBA$_{23}$)$_{42}$ have shown an encouraging dose-dependent silencing of the polo-like kinase 1 (PLK-1) gene, a well-known proto-oncogene, in a human renal carcinoma cell line (OSRC-2) with minimal cytotoxicity (Figure S3).

In summary, our results demonstrate that a PBA-functionalized PIC micelle can be used for intracellular ATP-triggered release of siRNAs. The window of concentrations over which complex stability can be controlled is ideal for further fine-tuning. The strength of the ribose–PBA binding and the hydrophobicity of PBA, both critical determinants of complex stability, as well as ATP sensitivity, are further controllable on the basis of the substituent group structures.[13,14,17] By varying the type and length of the counterpart polycations, improved biocompatibility and endosomal escape[21–23] could be acheived. Further efforts are being directed toward these possibilities, along with in vitro and in vivo studies of gene silencing.

Experimental Section

PEG-*b*-PLys was synthesized using a previously described method.[24] FPBA modification of lysine residue in the PEG-*b*-PLys$_{42}$ with different numbers of FPBA was performed by aqueous phase condensation reaction using 4-(4,6-dimethoxy-1,3,5-triazin-2-yl)-4-methylmorpholinium (DMT-MM). The resulting polymers (5 mg mL^{-1}) and siRNA (15 μM) were dissolved in HEPES buffered solution (HBS; 10 mM, pH 7.3). These were mixed in various N/P ratios to prepare the complexes. The cumulant diameter and zeta

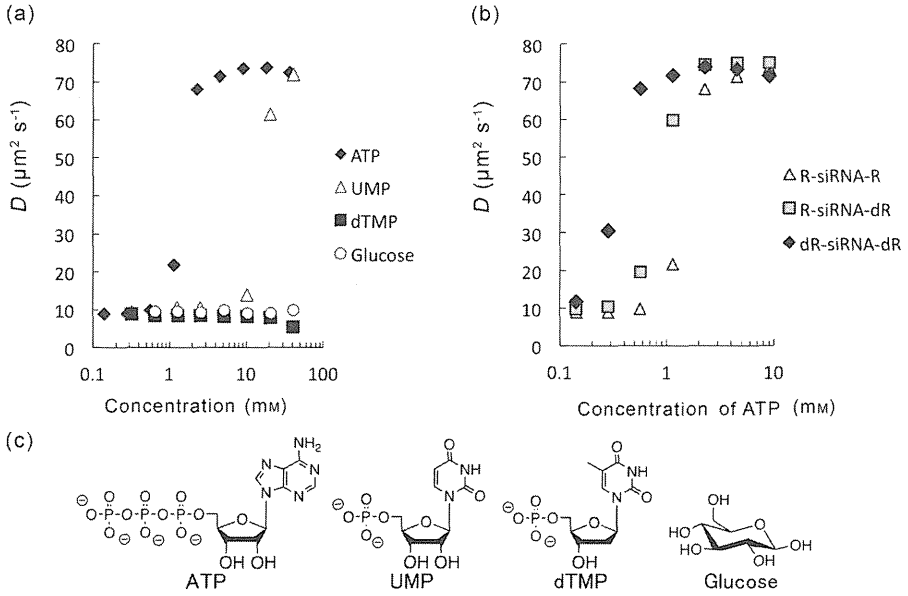

Figure 4. Ribose-specific stabilization of the complex and its sensitivity to a changing environment. a) Changes in the diffusion coefficient of Cy3-labeled siRNAs complexed with PEG-*b*-P(Lys/FPBA$_{23}$)$_{42}$ as a function of various additive concentrations after a 1 h incubation. b) Changes in the diffusion coefficient of siRNAs with different numbers of ribose functionalities when complexed with PEG-*b*-P(Lys/FPBA$_{23}$)$_{42}$ as a function of ATP concentration. c) Chemical formulas of the additives.

potential of the complexes were measured using a Zetasizer Nano (Malvern Instruments Ltd., Worcestershire, UK) after dilution with HBS to give 4 μM siRNA. To compare the siRNA loading ability of the FPBA modified polymers, siRNAs that were labeled with Cy3 at the 5′ end of the anti-sense strand were subjected to 1% agarose gel electrophoresis at 100 V for 20 min. The complexes with PEG-*b*-P(Lys/FPBA$_{19,23}$)$_{42}$ at N/P = 4 were diluted with HBS containing DSS at various A/P ratios to a final siRNA concentration of 50 nM and allowed to stand for 1 h at room temperature. To demonstrate the importance of ribose functionality at the 3′ end(s) of the siRNA, three types of siRNA-loaded micelles (R-siRNA-R, R-siRNA-dR, dR-siRNA-dR) were prepared from PEG-*b*-P(Lys/FPBA$_{23}$)$_{42}$ at various N/P ratios, diluted with HBS to be a final siRNA concentration of 50 nM, and allowed to stand for 1 h at room temperature before gel electrophoresis was performed. To demonstrate the stability of the micelles in serum, or with competitive monosaccharides or ribose, FCS analyses were conducted using an LSM-510-META equipped with FCS setup (ConfoCor3, Carl Zeiss Microscopy, Ltd.). For the stability test, the Cy3-labeled siRNA was complexed with PEG-*b*-P(Lys/FPBA$_{23}$)$_{42}$ at various N/P ratios, diluted with HBS or HBS containing 10% FBS to be a final siRNA concentration of 50 nM, and allowed to stand for 1 h at room temperature. For the ribose-resistance test, a complex of Cy3-labeled siRNA and PEG-*b*-P(Lys/FPBA$_{23}$)$_{42}$ at N/P = 4 was diluted with HBS containing various amount of ATP, UMP, dTMP, or glucose to be a final siRNA concentration of 50 nM and allowed to stand for 1 h at room temperature. FCS measurements were performed with a sampling time of 20 s at room temperature. The autocorrelation curves obtained from ten repeated measurements were converted to the diffusion time according to the manufacturer's instructions. Finally, the diffusion time was converted to the diffusion coefficient based on calibration using Rhodamine 6G.

More detailed information on materials, instruments, polymer synthesis, methods of complex characterization, complex stabilities in the absence of FBS, and an in vitro study of RNA interference is provided in the Supporting Information.

Received: May 2, 2012
Revised: June 26, 2012
Published online: August 21, 2012

Keywords: drug release · micelles · phenylboronic acid · polycations · siRNA

[1] K. A. Whitehead, R. Langer, D. G. Anderson, *Nat. Rev. Drug Discovery* **2009**, *8*, 129–138.
[2] N. Nishiyama, K. Kataoka, *Pharmacol. Ther.* **2006**, *112*, 630–648.
[3] M. Oishi, Y. Nagasaki, K. Itaka, N. Nishiyama, K. Kataoka, *J. Am. Chem. Soc.* **2005**, *127*, 1624–1625.
[4] K. Itaka, N. Nakayama, N. Nishiyama, W. D. Jang, Y. Yamasaki, K. Nakamura, H. Kawaguchi, K. Kataoka, *J. Am. Chem. Soc.* **2004**, *126*, 13612–13613.
[5] S. Matsumoto, R. J. Christie, N. Nishiyama, K. Miyata, A. Ishii, M. Oba, H. Koyama, Y. Yamasaki, K. Kataoka, *Biomacromolecules* **2009**, *10*, 119–127.
[6] a) D. B. Rozema, D. L. Lewis, D. H. Wakefield, S. C. Wong, J. J. Klein, P. L. Roesch, S. L. Bertin, T. W. Reppen, Q. Chu, A. V. Blokhin, J. E. Hagstrom, J. A. Wolf, *Proc. Natl. Acad. Sci. USA* **2007**, *104*, 12982–12987; b) M. Meyer, C. Dohmen, A. Philipp, D. Kiener, G. Maiwald, C. Scheu, M. Ogris, E. Wagner, *Mol. Pharm.* **2009**, *6*, 752–762.
[7] H. Mok, S. H. Lee, J. W. Park, T. G. Park, *Nat. Mater.* **2010**, *9*, 272–278.
[8] H. Takemoto, A. Ishii, K. Miyata, M. Nakanishi, M. Oba, T. Ishii, Y. Yamasaki, N. Nishiyama, K. Kataoka, *Biomaterials* **2010**, *31*, 8097–8105.
[9] A. Alshamsan, A. Haddadi, V. Incani, J. Samuel, A. Lavasanifar, H. Uludag, *Mol. Pharm.* **2009**, *6*, 121–133.
[10] W. J. Kim, L. V. Christensen, S. Jo, J. W. Yockman, J. H. Jeong, Y. H. Kim, S. W. Kim, *Mol. Ther.* **2006**, *14*, 343–350.
[11] H. J. Kim, A. Ishii, K. Miyata, Y. Lee, S. Wu, M. Oba, N. Nishiyama, K. Kataoka, *J. Controlled Release* **2010**, *145*, 141–148.
[12] R. J. Christie, K. Miyata, Y. Matsumoto, T. Nomoto, D. Menasco, T. C. Lai, M. Pennisi, K. Osada, S. Fukushima, N. Nishiyama, Y. Yamasaki, K. Kataoka, *Biomacromolecules* **2011**, *12*, 3174–3185.
[13] G. Springsteen, B. Wang, *Tetrahedron* **2002**, *58*, 5291–5300.
[14] J. Yan, G. Springsteen, S. Deeter, B. Wang, *Tetrahedron* **2004**, *60*, 11205–11209.
[15] N. Singh, R. C. Willson, *J. Chromatogr. A* **1999**, *840*, 205–213.
[16] E. Uğuzdoğan, E. B. Denkbaş, A. Tuncel, *Macromol. Biosci.* **2002**, *2*, 214–222.
[17] A. Matsumoto, R. Yoshida, K. Kataoka, *Biomacromolecules* **2004**, *5*, 1038–1045.
[18] M. Leist, B. Single, A. F. Castoldi, S. Kuhnle, P. Nicotera, *J. Exp. Med.* **1997**, *185*, 1481–1486.
[19] M. W. Gorman, E. O. Feigl, C. W. Buffington, *Clin. Chem.* **2007**, *53*, 318–325.
[20] T. W. Traut, *Mol. Cell. Biochem.* **1994**, *140*, 1–22.

[21] K. Miyata, M. Oba, M. Nakanishi, S. Fukushima, Y. Yamasaki, H. Koyama, N. Nishiyama, K. Kataoka, *J. Am. Chem. Soc.* **2008**, *130*, 16287 – 16294.
[22] N. Kanayama, S. Fukushima, N. Nishiyama, K. Itaka, W. D. Jang, K. Miyata, Y. Yamasaki, U. I. Chung, K. Kataoka, *ChemMedChem* **2006**, *1*, 439 – 444.
[23] H. Uchida, K. Miyata, M. Oba, T. Ishii, T. Suma, K. Itaka, N. Nishiyama, K. Kataoka, *J. Am. Chem. Soc.* **2011**, *133*, 15524 – 15532.
[24] M. Sanjoh, S. Hiki, Y. Lee, M. Oba, K. Miyata, T. Ishii, K. Kataoka, *Macromol. Rapid Commun.* **2010**, *31*, 1181 – 1186.

Journal of Controlled Release 161 (2012) 868–874

Contents lists available at SciVerse ScienceDirect

Journal of Controlled Release

journal homepage: www.elsevier.com/locate/jconrel

Pancreatic cancer therapy by systemic administration of VEGF siRNA contained in calcium phosphate/charge-conversional polymer hybrid nanoparticles

Frederico Pittella [a,b], Kanjiro Miyata [a], Yoshinori Maeda [b], Tomoya Suma [b], Sumiyo Watanabe [a], Qixian Chen [c], R. James Christie [a], Kensuke Osada [c], Nobuhiro Nishiyama [a], Kazunori Kataoka [a,b,c,d,*]

[a] Division of Clinical Biotechnology, Center for Disease Biology and Integrative Medicine, Graduate School of Medicine, The University of Tokyo, 7-3-1 Hongo, Bunkyo-ku, Tokyo 113-0033, Japan
[b] Department of Bioengineering, Graduate School of Engineering, The University of Tokyo, 7-3-1 Hongo, Bunkyo-ku, Tokyo 113-8656, Japan
[c] Department of Materials Engineering, Graduate School of Engineering, The University of Tokyo, 7-3-1 Hongo, Bunkyo-ku, Tokyo 113-8656, Japan
[d] Center for NanoBio Integration, The University of Tokyo, 7-3-1 Hongo, Bunkyo-ku, Tokyo 113-8656, Japan

ARTICLE INFO

Article history:
Received 16 February 2012
Accepted 1 May 2012
Available online 11 May 2012

Keywords:
siRNA
Calcium phosphate
Nanoparticle
VEGF
PEG
Charge-conversional polymer

ABSTRACT

Development of an efficient *in vivo* delivery vehicle of small interfering RNA (siRNA) is the key challenge for successful siRNA-based therapies. In this study, toward systemic delivery of siRNA to solid tumors, a smart polymer/calcium phosphate (CaP)/siRNA hybrid nanoparticle was prepared to feature biocompatibility, reversible stability and endosomal escape functionality using a pH sensitive block copolymer of poly(ethylene glycol) and charge-conversional polymer (PEG-CCP), of which anionic functional groups could be converted to cationic groups in an endosomal acidic condition for facilitated endosomal escape. Nanoparticles were confirmed to be approximately 100 nm in size, narrowly dispersed and spherical. Also, the nanoparticle was highly tolerable in medium containing serum, while releasing the entrapped siRNA in a cytoplasm-mimicking ionic condition, presumably based on the equilibrium between CaP complexes and calcium ions. Further, the nanoparticle showed high gene silencing efficiency in cultured pancreatic cancer cells (BxPC3) without associated cytotoxicity. Ultimately, systemic administration of the nanoparticles carrying vascular endothelium growth factor (VEGF) siRNA led to the significant reduction in the subcutaneous BxPC3 tumor growth, well consistent with the enhanced accumulation of siRNA and the significant VEGF gene silencing (~68%) in the tumor. Thus, the hybrid nanoparticle was demonstrated to be a promising formulation toward siRNA-based cancer therapies.

1. Introduction

Since elucidation of the molecular pathway of ribonucleic acid interference (RNAi) [1], small interfering ribonucleic acid (siRNA) has emerged as a potential therapeutic agent for modulating the production of proteins associated with disease [2,3]. Several clinical trials employing siRNA-based cancer therapies are currently ongoing [3,4]. In many cases, siRNA has been applied with a delivery vehicle to facilitate accumulation within the therapeutic site of activity (cell cytoplasm). Incorporation of siRNA within delivery vehicles is performed to overcome barriers associated with transport of this fragile and highly anionic macromolecule, such as premature degradation by RNases and inefficient cellular internalization. Therefore, development of more effective delivery vehicles is currently a major challenge for improving siRNA therapies.

Calcium phosphate (CaP)-based nanoparticles are a promising siRNA delivery platform because of the fact that CaP is naturally generated in the body (thus well tolerated), and also encapsulates negatively charged molecules during precipitation [5,6]. In this regard, a strategy to control the growth of CaP/siRNA precipitates is essential for their utilization toward systemic delivery applications. Several previous studies, including ours, have developed successful strategies to control nanoparticle size on the order of several tens to one hundred nanometer by coating with poly(ethylene glycol) (PEG)-*b*-polyanions [7–10], PEG-functionalized bisphosphonate [11], lipid bilayer membranes [12], or even nucleic acids [13]. Notably, a PEG shell on the nanoparticle surface has the desirable functionality to reduce non-specific interactions with biomacromolecules in the bloodstream, termed stealth property, for improved pharmacokinetics as well as facilitated accumulation in solid tumors through enhanced permeability and retention (EPR) effect [14–17].

Once internalized by cells via endocytosis, nanoparticles are transported to endosomal compartments ultimately lysosome where they remain until degraded. To overcome the endosomal/lysosomal entrapment of CaP nanoparticles, we developed CaP/polymer hybrid

* Corresponding author at: Division of Clinical Biotechnology, Center for Disease Biology and Integrative Medicine, Graduate School of Medicine, The University of Tokyo, 7-3-1 Hongo, Bunkyo-ku, Tokyo 113-0033, Japan.
E-mail address: kataoka@bmw.t.u-tokyo.ac.jp (K. Kataoka).

0168-3659/$ – see front matter © 2012 Elsevier B.V. All rights reserved.
doi:10.1016/j.jconrel.2012.05.005

nanoparticles containing functionality designed to promote escape from these subcellular compartments. This was achieved using a block copolymer of PEG and an endosome-disrupting polyanion, poly(*N*″-{*N*′-[(*N*-*cis*-aconityl)-2-aminoethyl]-2-aminoethyl}aspartamide) (PAsp(DET-Aco)) [18]. PAsp(DET-Aco) is relatively stable at the extracellular pH of 7.4 but degrades at pH ~5.5 (lysosome pH) by cleavage of *cis*-aconitic amide linkages, thus reverting back to the parent polycation, PAsp(DET). This degradation event results in conversion of the polymer charge from anionic to cationic, and is thus termed a charge-conversional polymer (CCP) (Fig. 1) [19]. PAsp(DET) has been shown to exhibit a distinctive change in the structure of side chains between pH 7.4 and pH 5.5 due to protonation of amino groups, i.e., monoprotonated diaminoethane at pH 7.4 and diprotonated diaminoethane at pH 5.5, allowing pH-selective membrane disruption for efficient endosomal escape of nucleic acids without associated toxicity [20–25]. In addition, PEG-PAsp(DET-Aco) was confirmed to facilitate excellent colloidal dispersion of CaP nanoparticles, while also improving the endosomal escape of siRNA, resulting in efficient gene silencing to cultured pancreatic carcinoma cells (PanC-1) [18].

The present work reports the *in vivo* application of the CaP/block copolymer/siRNA hybrid nanoparticles prepared with PEG-PAsp(DET-Aco) for treatment of subcutaneous pancreatic tumor (BxPC3) models in mice by systemic administration. Removal of free calcium ions from CaP nanoparticle solutions is critical for its systemic administration, as excess calcium ions may induce adverse effects in the bloodstream [32]. Thus nanoparticle solutions were purified by ultrafiltration, and then characterized with non-purified controls in terms of stability, morphology, calcium amount and biological activity. For treatment of subcutaneous pancreatic tumors, the key pro-angiogenic molecule vascular endothelial growth factor (VEGF) was selected as the target gene, once it is known to be over-expressed in many cancerous cells, promoting angiogenesis through endothelial proliferation, survival and migration [26]. Moreover, silencing of the VEGF signaling pathway has been shown to suppress tumor angiogenesis and growth [27–30]. After systemic administration of purified nanoparticles incorporating VEGF siRNA for anti-angiogenic therapy, the accumulation of siRNA and the expression level of VEGF mRNA in the tumor tissue were evaluated to elucidate their correlation with tumor growth rates. This work demonstrates significant antitumor activity induced by VEGF gene silencing with siRNA delivered by CaP/block copolymer hybrid nanoparticles.

2. Materials and methods

2.1. Materials, cell line and animals

Dulbecco's modified eagle's medium (DMEM) without L-glutamine and phenol red, RPMI 1640 and *cis*-aconitic anhydride were purchased from Sigma-Aldrich (St. Louis, MO). α-Methoxy-ω-amino poly(ethylene glycol) (MeO–PEG–NH_2) (M_w: 12,000) and β-benzyl-L-aspartate *N*-carboxy anhydride (BLA-NCA) were obtained from NOF Co., Inc. (Tokyo, Japan) and Chuo Kaseihin Co., Inc. (Tokyo, Japan), respectively. *N*-methyl-2-pyrrolidone (NMP), diethylenetriamine (DET), dimethyl sulfoxide (DMSO), *N*,*N*-dimethylformamide (DMF), dichloromethane (DCM) and acetic anhydride were purchased from Tokyo Chemical Industry Co. Ltd. (Tokyo, Japan) or Nacalai Tesque (Tokyo, Japan), and used after conventional distillation. Acetic acid, acetonitrile, acetone, diethyl ether and hydrochloric acid were purchased from Wako Pure Chemical Industries Ltd. (Osaka, Japan). Fetal bovine serum (FBS) was purchased from Dainippon Sumitomo Pharma Co., Ltd. (Osaka, Japan). RT-PCR primers used for human actin and human VEGF were synthesized by Hokkaido System Science (Hokkaido, Japan) and the sequences are the following: CCAACCGCGAGAAGATGA (actin forward); CCAGAGGCGTACAGGGATAG (actin reverse); AGTGGTCCCAGGCTGCAC (VEGF forward); TCCATGAACTTCACCACTTCGT (VEGF reverse). All the siRNAs were synthesized by Hokkaido System Science (Hokkaido, Japan). The sequences of VEGF siRNA (siVEGF) are 5′-GGAGUACCCUGAUGAGAUCdTdT-3′ (sense) and 5′-GAUCUCAUCAGGGUACUCCdTdT-3′ (antisense), and the sequences of scramble siRNA (siSCR) are 5′-UUCUCCGAACGUGUCACGUdTdT-3′ (sense); 5′-ACGUGACACGUUCGGAGAAdTdT-3′ (antisense).

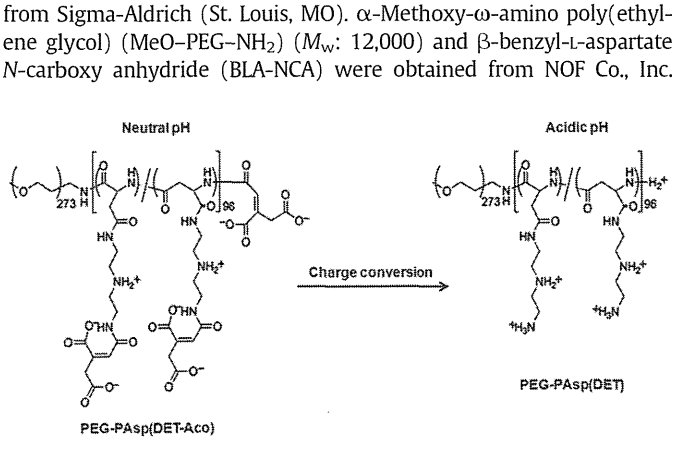

Fig. 1. Change in the chemical structure of PEG-PAsp(DET-Aco) to PEG-PAsp(DET) in response to the acidic pH.

BxPC3 cells (human tumorigenic pancreatic adenocarcinoma, ATCC number: CRL-1687) were obtained from the American Type Culture Collection (Manassas, VA). Cells were maintained in RPMI 1640 medium (Sigma Chemical Co., Inc.) containing 10% fetal bovine serum (FBS) in a humidified atmosphere containing 5% CO_2 at 37 °C. Balb-c nu/nu mice (female; 18–20 g body weight; age, 6 weeks) were purchased from Charles River Japan (Kanagawa, Japan). All animal experiments were performed in accordance with the Guidelines for the Care and Use of Laboratory Animals as stated by the University of Tokyo.

2.2. Polymer synthesis

Detailed synthesis methods of the parent polycation PEG-PAsp(DET) and PEG-PAsp(DET-Aco) derivative are described in Supplementary data.

2.3. Preparation of PEG-CCP/siRNA/CaP hybrid nanoparticles

A solution of 2.5 M $CaCl_2$ (1 μL) was diluted in 10 mM Tris buffer (pH 10) (11.5 μL). Another solution containing PEG-PAsp(DET-Aco) (1.0 mg/mL) in 10 mM Tris/HCl buffer (pH 7.5) was mixed with a solution of 15 μM siRNA in 10 mM HEPES buffer (pH 7.2) and with 50 mM HEPES buffer containing 1.5 mM Na_3PO_4 and 140 mM NaCl (pH 7.5) (2.5 μL: 5 μL: 5 μL). The former solution was mixed with the latter solution by pipetting for around 20 s (final siRNA concentration; 3 μM).

2.4. Purification of PEG-CCP/siRNA/CaP hybrid nanoparticles

The purification of hybrid nanoparticles for removal of excess amount of free calcium ions was carried out immediately after preparation. PEG-CCP/siRNA/CaP hybrid nanoparticle solution containing 41.3 μg siRNA and 150 μg PEG-CCP (1 mL) was added to a VivaSpin-06 device (MWCO: 10 kDa) containing 1 mL of an extracellular (EC) buffer that mimics the ionic strength of extracellular environment (2 mM $CaCl_2$, 1 mM Na_2HPO_4, 25 mM Tris and 140 mM NaCl at pH 7.4) [8]. The mixture was centrifuged in a swing bucket rotor at 900 g and 4 °C for 20 min. To minimize non-specific binding of nanoparticles to the membrane, the centrifuge filter devices were washed with de-ionized water before use. After centrifugation, the retained solution was collected and used in further experiments.

2.5. Determination of calcium content in nanoparticles

The total calcium content present in the solution of non-purified and purified/concentrated hybrid nanoparticles was determined by the SRL Laboratories (SRL Inc., Tokyo, Japan) through spectrophotometry using

arsenazo III. All the samples were diluted four times with distilled water to the final volume of 300 μL before assay. The reaction of arsenazo III dye with calcium under acidic conditions produces a blue–purple complex, of which concentration is determined spectrophotometrically at the wavelength of 660 nm. Obtained values were used to calculate the efficiency of calcium removal from nanoparticle solution.

2.6. Dynamic light scattering (DLS) measurements

DLS measurements were carried out at 25 °C using a Zetasizer Nano ZS (Malvern Instruments, UK) at a detection angle of 173° with a He–Ne laser (633 nm) as the incident beam. The data obtained from the rate of decay in the photon correlation function were analyzed with a cumulant method to obtain the corresponding hydrodynamic diameters and polydispersity indices (PdI) (μ/G^2) of the nanoparticles. The colloidal stability of both purified and non-purified nanoparticles was monitored during several days and the result was presented as a relative size to the initial hydrodynamic diameter obtained in the first day.

2.7. Atomic force microscopy (AFM) imaging

AFM imaging of the nanoparticles was performed using a MMAFM, Nanoscope V (Bruker AXS, Madison, WI) in ScanAsyst Atomic Force Microscopy Imaging mode with standard silicon probes. Imaging was conducted under air on a highly orientated pyrolytic graphite (HOPG) substrate. The obtained images were processed by flattening to remove the background slope of the substrate surface.

2.8. Fluorescence correlation spectroscopy (FCS) measurements

FCS measurements were performed using a Confocor3 module (Carl Zeiss, Jena, Germany) equipped with a Zeiss C-Apochromat 40× water objective. Samples prepared with Cy5-labeled siRNA were measured with the excitation of a He–Ne laser (633 nm, 5 mW) and the emission passed through a 650 nm long pass filter. Samples were placed into 8-well Lab-Tek chambered borosilicate cover-glass slides (Nalge Nunc International, Rochester, NY). Determination of the focal volume was established by calibration with 10 nM Cy5 standard solution. Each analysis consisted of 10 measurements with a sampling time of 20 s and the measured autocorrelation curves were fitted with the Zeiss Confocor3 software package to obtain the diffusion coefficient. The stability of nanoparticles under a cell culture condition was evaluated after dilution of samples with DMEM containing 10% FBS without L-glutamine and phenol red and then incubation at 37 °C. The stability of nanoparticles in the solution mimicking the intracellular fluids was evaluated after dilution of the samples with the ionic solution ($CaCl_2$ 100 nM, Na_2HPO_4 40 mM, NaCl 140 mM, pH 7.4), as previously described [8]. The concentration of Cy5-labeled siRNA was adjusted to 100 nM, corresponding to the *in vitro* gene silencing experiment.

2.9. In vitro gene silencing

To evaluate the gene silencing efficiency of the purified nanoparticles compared to non-purified controls, BxPC3 cells were seeded with 2 mL of RPMI 1640 containing 10% FBS on a 6 well plate at 5×10^4 cells/well. After 24 h, nanoparticle solutions were added with fresh medium (100 nM siRNA). After another 24 h, cells were harvested and RNA was extracted using RNeasy Mini Kit (Qiagen, Valencia, CA), according to the manufacturer's instruction.

2.10. Real-time reverse transcriptional (RT)-PCR

After obtaining the RNA from cells or tissue, the RNA concentration was measured and then sample concentrations were normalized. Next, the genomic DNA elimination was performed prior to cDNA synthesis using a QuantiTect Reverse Transcription kit (Qiagen, Valencia, CA). Real-time RT-PCR was performed using an ABI 7500 Fast Real-time RT-PCR System (Applied Biosystems, Foster City, CA) and QuantiTect SYBR Green PCR Master Mix (Qiagen, Valencia, CA). Actin was used as the house-keeper gene and the obtained data were normalized before statistical analysis.

2.11. Antitumor activity

Balb/c nude mice (female, 6 week old) were subcutaneously implanted with BxPC3 tumor (3 mm×3 mm×1 mm). The tumors were allowed to grow for 3 weeks before sample injection. Further, the mice bearing tumors with similar volume (~50 mm^3) were randomly distributed in groups ($n=4$). Thereafter, hybrid nanoparticles loading siVEGF (25 μg siRNA in 200 μL per injection) were injected into the tail vein 4 times at days 2, 5, 8 and 12. Tumor size and body weight for each mouse were monitored for 13 days. The tumor volume was calculated based on a modified ellipsoidal formula [30,31]: tumor volume = $1/2(\text{length}\times\text{width}^2)$.

2.12. Tumor accumulation

Similarly to Section 2.11, BxPC3 tumor-bearing mice were prepared by subcutaneous implantation of the tumor pieces (3 mm×3 mm×1 mm). The tumors were allowed to grow for 4 weeks before sample injection. Five mice bearing tumors of the similar volume (~70 mm^3) were randomly selected for each cohort ($n=5$). Hybrid nanoparticles containing Cy5-labeled siRNA were intravenously injected into the tail vein at 15 μg of Cy5-labeled siRNA per injection. Mice were sacrificed 60 min after injection and tumors were excised. Cy5 fluorescence from the tumor tissue was measured by IVIS (Caliper Life Sciences, Hopkinton, MA). Results were expressed as total photon counts normalized by tumor weight.

2.13. In vivo gene silencing in tumor tissue

BxPC3 tumor-bearing mice were prepared by subcutaneous implantation of the tumor pieces (3 mm×3 mm×1 mm) and then allowed to grow for 4 weeks, similar to the method described in Sections 2.11 and 2.12. Mice bearing tumors of similar volume (~70 mm^3) were randomly distributed in groups ($n=3$). Thereafter, hybrid nanoparticles loading siVEGF (25 μg siRNA in 200 μL per injection) were injected into the tail vein on days 1, 4, 8 and 34. After 24 h of the last injection, each tumor was excised and the non-necrotic part of the tumor (~20 mg) was cut into small pieces and sonicated for 10 s in a lysis buffer. The lysate was centrifuged and then the supernatant was used to extract RNA using the RNeasy Mini Kit (Qiagen, Valencia, CA), according to the manufacturer's instruction. Extracted RNA was further used to verify VEGF gene silencing by real-time RT-PCR, as described in Section 2.10.

3. Results and discussion

3.1. Preparation and purification/concentration of hybrid nanoparticles

The functional CCP block copolymer, PEG-PAsp(DET-Aco) (Fig. 1), was synthesized using a procedure similar to our previous report [18]. Successful synthesis of PEG-PAsp(DET-Aco) was confirmed from the ^{1}H NMR spectrum (Supporting Fig. 1) by the appearance of protons present on acid-labile *cis*-aconitic amide (Aco) moieties. This introduction is accompanied by the conversion of cationic charges to negative charges in the polyaspartamide side chain, enabling integration of PEG-CCP into CaP nanoparticles. The prepared charge-conversional polymer shows high stability at neutral pH but becomes cleavable at acidic pH to reproduce cationic PAsp(DET) from anionic PAsp(DET-Aco) (Fig. 1). Note that, once in the acidic environment of the endosome/lysosome, PAsp(DET) can disrupt their membrane to facilitate the escape of nanoparticles from these compartments [18,25].

PEG-CCP/CaP hybrid nanoparticles were prepared by simple mixing of the component solutions [18]. The initial solution of the prepared nanoparticles contains several ions, such as Ca^{2+}, that may perturb the normal body homeostasis when applied systemically [32], thereby requiring purification of the solution for removal of the ions before systemic administration. However, the CaP nanoparticles are likely to dissociate in lower ionic strength solutions due to an equilibrium shift [8–10]. Thus, a suitable buffer solution is necessary for maintaining nanoparticle structure after purification. Our previous work suggested that PEGylated CaP nanoparticles were tolerable to an extracellular ionic solution ($CaCl_2$ 2 mM, Na_2HPO_4 1 mM, Tris 25 mM, NaCl 140 mM, pH 7.4) as they effectively delivered siRNA into cultured cells in that solution. The calcium concentration of the extracellular ionic solution is similar to that of body fluids, suggesting that minimal perturbation to blood homeostasis following intravenous administration is expected.

Hybrid nanoparticle solutions were purified by an ultrafiltration method, which allows rapid exchange of the buffer solutions. The ultrafiltration (MWCO: 10 kDa) was performed with replacement of the original solution for nanoparticle preparation ($CaCl_2$ 100 mM, Na_3PO_4 0.3 mM, NaCl 28 mM, Tris 6.6 mM, HEPES 12 mM) with EC buffer ($CaCl_2$ 2 mM, Na_2HPO_4 1 mM, Tris 25 mM, NaCl 140 mM, pH 7.4). The arsenazo III dye-based colorimetric assay revealed that the ultrafiltration process removed 84% of the original calcium content, with residual calcium corresponding mostly to the calcium contained in nanoparticles. The resulting nanoparticles were characterized by DLS and AFM. Purified nanoparticles maintained a narrowly dispersed size distribution in the DLS (Z-weighted) histogram, similar to non-purified controls (Fig. 2A). Spherical morphologies with the similar size were observed in the AFM images of both purified and non-purified hybrid nanoparticles (Figs. 2B and C). These results indicate that purification for removal of excess calcium ions was successful, without alteration of hybrid nanoparticle structure.

Hybrid nanoparticle stability upon storage is also important for their quality control towards pharmaceutical applications. Thus, the size of hybrid nanoparticle was monitored over time by DLS following storage at 4 °C (Fig. 3). Non-purified hybrid nanoparticles did not show a significant change in both size and PdI for at least 168 h (7 days). Purified nanoparticle size remained similar to that of the non-purified control for the first 96 h and then the size slightly increased thereafter, possibly due to secondary aggregate formation. This aggregation can be explained by compromised colloidal stability of nanoparticles, triggered by PEG-CCP detachment from the nanoparticles associated with their gradual dissolution. These results suggest that the dissolution of the purified nanoparticle is intrinsically slow in the EC buffer.

3.2. Stability of hybrid nanoparticles in a serum-containing culture medium and a cytoplasmic ionic solution

Purified hybrid nanoparticle stability was further assessed in medium containing serum proteins. Nanoparticles were prepared with Cy5-labeled siRNA (Cy5-siRNA) and then subjected to fluorescence correlation spectroscopy (FCS) analysis. FCS analysis allows determination of the diffusion coefficient of siRNA-incorporating nanoparticles in the complex protein-containing solution without interference from non-labeled macromolecules or aggregates [33–35]. Note that the diffusion coefficient is inversely proportional to the hydrodynamic size of the fluorescent molecule based on the Stokes–Einstein equation for spherical particles; thus the size of nanoparticles can be determined. In conventional condition used for siRNA transfection (100 nM siRNA in 10% FBS medium), the initial size of nanoparticles was determined to be approximately 100 nm (Fig. 4A), which is consistent with the size in DLS histogram and AFM image of nanoparticles not exposed to biological media (Fig. 2). Additionally, size was maintained following 4 h incubation at 37 °C, indicating high tolerability in medium containing serum proteins.

In addition to high tolerability within extracellular conditions, delivery vehicles must finally release the encapsulated siRNA in the cytoplasm to gain access to the RNAi pathway. Hence, siRNA release from the hybrid nanoparticles was further evaluated by FCS in a solution mimicking the ionic condition of the cytoplasm ($CaCl_2$ 100 nM, Na_2HPO_4 40 mM, NaCl 140 mM, pH 7.4), as the dissolution of CaP nanoparticles should be significantly influenced by the concentration of calcium and phosphate ions. The average calcium ion concentrations are 2 mM and 100 nM in the blood and the cytoplasm, respectively. The lower calcium concentration in the cell cytoplasm may trigger selective intracellular release of siRNA from the CaP nanoparticles. Indeed, when nanoparticles were incubated in the cytoplasmic ionic solution, the size of the nanoparticles was drastically reduced within 1 h incubation, ultimately reaching the same value of naked siRNA (Fig. 4B), which is consistent with our previous findings regarding the dissolution behavior of hybrid nanoparticles [8].

3.3. In vitro gene silencing

The gene silencing activity of nanoparticles containing siVEGF was evaluated in cultured human pancreatic adenocarcinoma (BxPC3) cells. BxPC3 was chosen as a target cancer cell because of the fact that subcutaneous BxPC3 tumors exhibit poorly differentiated histology with thick fibrotic stromal tissue surrounding tumor nests [36], thereby resembling intractable tumors in clinical settings. As shown in Fig. 5, both non-purified and purified hybrid nanoparticles encapsulating siVEGF significantly reduced VEGF mRNA in comparison with controls incorporating siSCR. The reduction in VEGF mRNA was 71% and 63% for purified and non-purified nanoparticles, respectively. Strong gene silencing activity of hybrid nanoparticles is probably due to their high complex stability in the transfection medium (Fig. 4A) and selective siRNA release in the cell cytoplasm (Fig. 4B) as well as facilitated endosomal escape of siRNA by PEG-CCP, as extensively examined in previous studies [18,19]. No statistical difference was found between nanoparticle formulations, indicating that there was apparently no loss of the biological activity of siRNA after purification. Analysis of cell viability (CCK-8, Dojindo, Japan) showed no difference between nanoparticle-treated samples and controls at tested siRNA

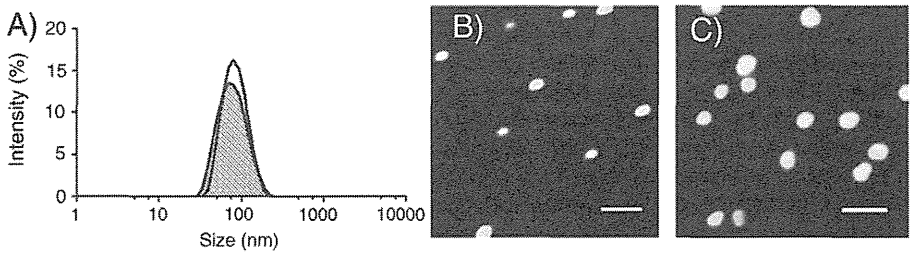

Fig. 2. (A) Size distribution of CaP nanoparticles before (filled curve) and after (open curve) purification by ultrafiltration, determined by DLS. (B, C) Atomic force microscopic images of non-purified (B) and purified (C) hybrid nanoparticles. Scale bar corresponds to 200 nm.

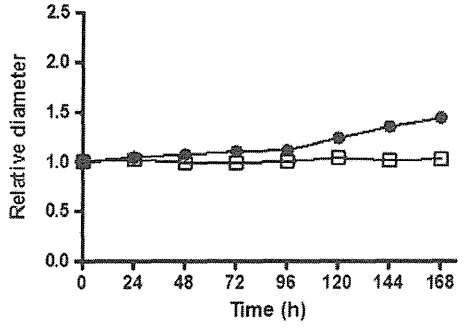

Fig. 3. Time-dependent change in the relative diameter of non-purified (open square) and purified (closed circle) hybrid nanoparticles, determined by DLS (temperature: 4 °C, siRNA concentration: 3 μM).

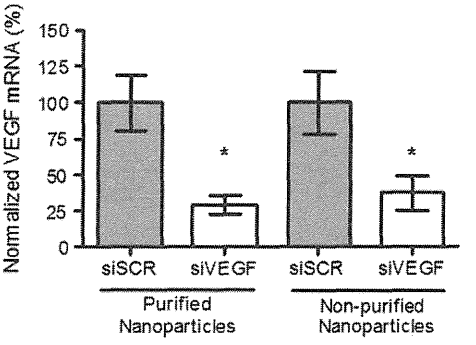

Fig. 5. Gene silencing activity of hybrid nanoparticles in cultured BxPC3 cells (siRNA concentration: 100 nM, incubation time: 24 h, $n=3$). *$p<0.05$ for the control incorporating siSCR (ANOVA followed by Newman–Keuls).

concentration (Supporting Fig. 2), indicating that VEGF silencing is due to the RNAi effect and not an artifact of toxicity.

3.4. Antitumor activity

Antitumor activity of siVEGF-incorporating hybrid nanoparticles was evaluated against a subcutaneous BxPC3 tumor model. Silencing of VEGF gene in tumor tissues can prevent angiogenesis, subsequently blocking the nutrient supply needed for tumor growth (antiangiogenic therapy). As presented in Fig. 6, tumors treated by I.V. injection of nanoparticles containing siVEGF showed suppressed growth, compared to those treated with nanoparticles containing siSCR as well as nanoparticles without siRNA and EC buffer only. A statistical significance was observed at days 3, 5, 7 and 9 for tumors treated with the siVEGF nanoparticles compared to controls. It is noteworthy that the significant tumor growth inhibition was observed after the first injection of the siVEGF nanoparticle. At day 9, the tumor volume in mice treated with the siVEGF nanoparticles was around 66% of the average volume of controls. I.V. injection of nanoparticles did not result in acute or severe toxicity, as no significant difference in body weight was observed between treated and control groups during the experimental period (data not shown). Additionally, blood levels of alanine aminotransferase (ALT) and aspartate aminotransferase (AST) were not significantly altered after I.V. injection of hybrid nanoparticles (Supporting Fig. 3), suggesting negligible acute toxicity associated with nanoparticle administration. These results demonstrate that the PEG-CCP/CaP hybrid nanoparticle with siVEGF is a promising formulation for cancer therapy.

3.5. Accumulation of siRNA and gene silencing in tumors

In order to obtain further evidence that the antitumor activity of siRNA-containing hybrid nanoparticles was induced by the RNAi effect, accumulation of siRNA within subcutaneous tumors was evaluated. Hybrid nanoparticles were prepared with Cy5-siRNA and injected into mice in the similar manner used for tumor growth inhibition experiments. Mice were sacrificed and the tumors were excised 60 min after systemic administration of the hybrid nanoparticles, and Cy5 fluorescence was measured by IVIS. Fluorescence intensity was normalized to the tumor weight for quantitative evaluation. Significantly stronger fluorescence was detected in tumors treated with hybrid nanoparticles, compared to naked siRNA (Fig. 7A), indicating enhanced tumor accumulation of siRNA by hybrid nanoparticle delivery. Considering the fact that naked siRNA is immediately degraded in the bloodstream and subsequently cleared from kidney, the improved tumor accumulation may be due to suppressed siRNA degradation in the bloodstream as well as slower renal clearance of siRNA.

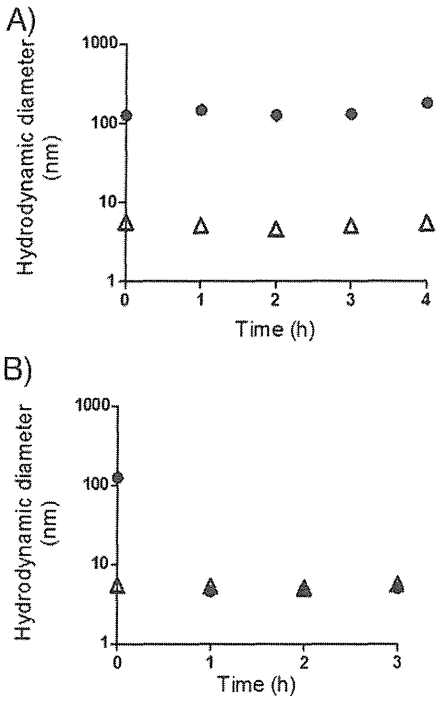

Fig. 4. Time-dependent change in hydrodynamic diameters of hybrid nanoparticles incorporating Cy5-siRNA (closed circle) and naked Cy5-siRNA (open triangle) determined by FCS in the medium containing 10% FBS (A) and in the medium mimicking the cytoplasm (Ca^{2+} and PO_4^{3-} concentrations were 100 nM and 40 mM, respectively) (B).

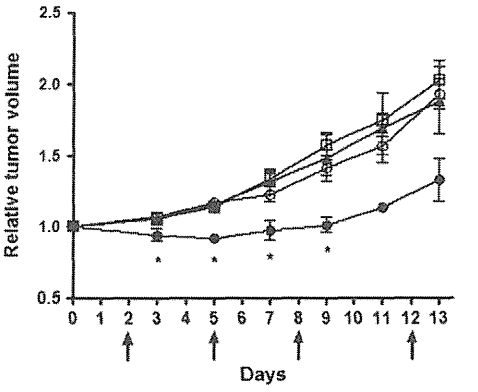

Fig. 6. Relative tumor volume of subcutaneous BxPC3 tumors treated by the hybrid nanoparticles with siVEGF (closed circle), with siSCR (closed triangle), hybrid nanoparticles without siRNA (open square) and EC buffer control (open circle) ($n=4$). Arrows indicate injection day (25 μg siRNA/injection). *$p<0.05$ for EC buffer control (ANOVA followed by Newman–Keuls).

Target gene mRNA levels were also evaluated as direct evidence for RNAi-based antitumor activity. In order to confirm VEGF mRNA degradation in tumor tissue, an additional injection of nanoparticles was performed to a separated group of mice bearing subcutaneous BxPC3 tumors ($n=3$). Approximately 1 day after the injection, mice were sacrificed and tumors were excised, followed by the extraction of RNA and real-time RT-PCR analysis. Fig. 7B clearly shows that significantly higher gene silencing activity (~68%) was achieved with hybrid nanoparticles containing siVEGF, compared to those prepared with siSCR as well as a buffer control. This result corroborates with the significant antitumor activity achieved with nanoparticles containing siVEGF (Fig. 6). Altogether, effective tumor accumulation and VEGF mRNA degradation strongly suggest that tumor growth suppression was a result of RNAi.

4. Conclusion

In this work, the *in vivo* application of PEG-CCP/CaP hybrid nanoparticles carrying siRNA was investigated for siRNA-based cancer treatment. Hybrid nanoparticles were submitted to purification for significant reduction of the amount of free calcium in solution. Purified hybrid nanoparticles were found to have the following characteristics: i) a similar size distribution and morphology to non-purified controls, ii) excellent tolerability in the serum-containing medium, iii) reversible capture of siRNA, with release in cytoplasmic ionic conditions. Efficient gene silencing activity without associated toxicity was also confirmed for nanoparticles in cultured BxPC3 cells. Intravenously injected nanoparticles incorporating VEGF siRNA led to significant reduction in tumor growth. Enhanced siRNA accumulation in subcutaneous BxPC3 tumors was found and subsequently induction of effective VEGF gene silencing in the tumor was observed. Based on the presented results, the PEG-CCP/CaP hybrid nanoparticles demonstrate great potential for clinical applications toward siRNA-based cancer therapies.

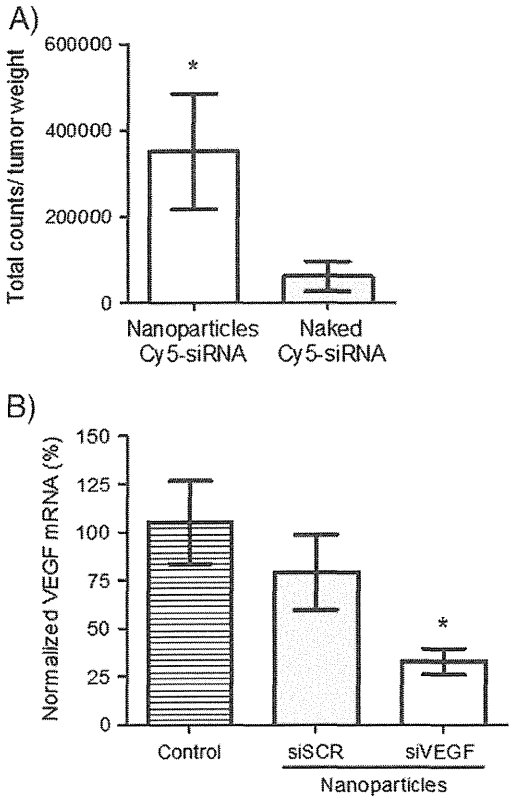

Fig. 7. (A) Accumulation of Cy5-siRNA in subcutaneous BxPC3 tumors 60 min after systemic administration. The Cy5 fluorescence intensity in the excised tumor tissue was determined by IVIS, followed by the normalization by the tumor weight ($n=5$). $^*p<0.05$ for naked Cy5-siRNA (Mann–Whitney t test). (B) *In vivo* VEGF gene silencing activity in subcutaneous BxPC3 tumors 1 day after systemic administration of samples (25 μg siRNA), revealed by real-time RT-PCR ($n=3$). $^*p<0.05$ for ionic buffer control (ANOVA followed by Newman–Keuls).

Acknowledgment

This research was granted by the Japan Society for the Promotion of Science (JSPS) through the "Funding Program for World-Leading Innovative R&D on Science and Technology (FIRST Program)," initiated by the Council for Science and Technology Policy (CSTP). The authors express their appreciation to Dr. M. Oba (Nagasaki University) and Dr. H. Cabral (The University of Tokyo) for the help in animal experiments.

Appendix A. Supplementary data

Supplementary data to this article can be found online at http://dx.doi.org/10.1016/j.jconrel.2012.05.005.

References

[1] A. Fire, S. Xu, M.K. Montgomery, S.A. Kostas, S.E. Driver, C.C. Mello, Potent and specific genetic interference by double-stranded RNA in *Caenorhabditis elegans*, Nature 391 (1998) 806–811.
[2] S.M. Elbashir, J. Harborth, W. Lendeckel, A. Yalcin, K. Weber, T. Tushl, Duplexes of 21-nucleotide RNAs mediate interference in cultured mammalian cells, Nature 411 (2001) 494–498.
[3] B.L. Davidson, P.B. McCray, Current prospects for RNA interference-based therapies, Nat. Rev. Genet. 12 (2011) 329–340.
[4] M.E. Davis, J.E. Zuckerman, C.H.J. Choi, D. Seligson, A. Tolcher, C.A. Alabi, Y. Yen, J.D. Heidel, A. Ribas, Evidence of RNAi in humans from systemically administered siRNA via targeted nanoparticles, Nature 464 (2010) 1067–1070.
[5] A. Maitra, Calcium phosphate nanoparticles: second-generation nonviral vectors in gene therapy, Expert. Rev. Mol. Diagn. 5 (2005) 893–905.
[6] M. Zhang, K. Kataoka, Nano-structured composites based on calcium phosphate for cellular delivery of therapeutic and diagnostic agents, Nano Today 4 (2009) 508–517.
[7] Y. Kakizawa, K. Kataoka, Block copolymer self-assembly into monodispersive nanoparticles with hybrid core of antisense DNA and calcium phosphate, Langmuir 18 (2002) 4539–4543.
[8] Y. Kakizawa, S. Furukawa, K. Kataoka, Block copolymer-coated calcium phosphate nanoparticles sensing intracellular environment for oligodeoxynucleotide and siRNA delivery, J. Control. Release 97 (2004) 345–356.
[9] Y. Kakizawa, S. Furukawa, A. Ishii, K. Kataoka, Organic–inorganic hybrid-nanocarrier of siRNA constructing through the self-assembly of calcium phosphate and PEG-based block aniomer, J. Control. Release 111 (2006) 368–370.
[10] M. Zhang, A. Ishii, N. Nishiyama, S. Matsumoto, T. Ishii, Y. Yamasaki, K. Kataoka, PEGylated calcium phosphate nanocomposites as smart environment-sensitive carriers for siRNA delivery, Adv. Mater. 21 (2009) 3520–3525.
[11] E.V. Giger, J. Puigmartí-Luis, R. Schlatter, B. Castagner, P.S. Dittrich, J.C. Leroux, Gene delivery with bisphosphonate-stabilized calcium phosphate nanoparticles, J. Control. Release 150 (2011) 87–93.
[12] J. Li, Y.C. Chen, Y.C. Tseng, C. Mozumdar, L. Huang, Biodegradable calcium phosphate nanoparticle with lipid coating for systemic siRNA delivery, J. Control. Release 142 (2010) 416–421.
[13] V.V. Sokolova, I. Radtke, R. Heumann, M. Epple, Effective transfection of cells with multi-shell calcium phosphate DNA nanoparticles, Biomaterials 27 (2006) 3147–3153.
[14] Y. Matsumura, H. Maeda, A new concept for macromolecular therapeutics in cancer-chemotherapy: mechanisms of tumoritropic accumulation of proteins and the antitumor agent SMANCS, Cancer Res. 46 (1986) 6387–6392.
[15] S.M. Moghimi, A.C. Hunter, J.C. Murray, Long-circulating and target-specific nanoparticles: theory to practice, Pharm. Rev. 53 (2001) 283–318.
[16] K. Kataoka, A. Harada, Y. Nagasaki, Block copolymer micelles for drug delivery: design, characterization and biological significance, Adv. Drug Deliv. Rev. 47 (2001) 113–131.
[17] K. Miyata, R.J. Christie, K. Kataoka, Polymeric micelles for nano-scale drug delivery, React. Funct. Polym. 71 (2011) 227–234.
[18] F. Pittella, M. Zhang, Y. Lee, H.J. Kim, T. Tockary, K. Osada, T. Ishii, K. Miyata, N. Nishiyama, K. Kataoka, Enhanced endosomal escape of siRNA-incorporating hybrid nanoparticles from calcium phosphate and PEG-block charge-conversional polymer for efficient gene knockdown with negligible cytotoxicity, Biomaterials 32 (2011) 3106–3114.
[19] Y. Lee, K. Miyata, M. Oba, T. Ishii, S. Fukushima, M. Han, H. Koyama, N. Nishiyama, K. Kataoka, Charge-conversional ternary polyplex with endosome disruption moiety: a technique for efficient and safe gene delivery, Angew. Chem. Int. Ed. 47 (2008) 5163–5166.
[20] N. Kanayama, S. Fukushima, N. Nishiyama, K. Itaka, W.D. Jang, K. Miyata, Y. Yamasaki, U.I. Chung, K. Kataoka, A PEG-based biocompatible block catiomer with high buffering capacity for the construction of polyplex micelles

showing efficient gene transfer toward primary cells, ChemMedChem 1 (2006) 439–444.
[21] K. Miyata, M. Oba, M. Nakanishi, S. Fukushima, Y. Yamasaki, H. Koyama, N. Nishiyama, K. Kataoka, Polyplexes from poly(aspartamide) bearing 1,2-diaminoethane side chains induce pH-selective, endosomal membrane destabilization with amplified transfection and negligible cytotoxicity, J. Am. Chem. Soc. 130 (2008) 16287–16294.
[22] S. Takae, K. Miyata, M. Oba, T. Ishii, N. Nishiyama, K. Itaka, Y. Yamasaki, H. Koyama, K. Kataoka, PEG-detachable polyplex micelles based on disulfide-linked block catiomers as bioresponsive nonviral gene vectors, J. Am. Chem. Soc. 130 (2008) 6001–6009.
[23] K. Itaka, T. Ishii, Y. Hasegawa, K. Kataoka, Biodegradable polyamino acid-based polycations as safe and effective gene carrier minimizing cumulative toxicity, Biomaterials 31 (2010) 3707–3714.
[24] H. Uchida, K. Miyata, M. Oba, T. Ishii, T. Suma, K. Itaka, N. Nishiyama, K. Kataoka, Odd-even effect of repeating aminoethylene units in the side chain of N-substituted polyaspartamides on gene transfection profiles, J. Am. Chem. Soc. 133 (2011) 15524–15532.
[25] K. Miyata, N. Nishiyama, K. Kataoka, Rational design of smart supramolecular assemblies for gene delivery: chemical challenge in the creation of artificial viruses, Chem. Soc. Rev. 41 (2012) 2562–2574.
[26] N. Ferrara, VEGF as a therapeutic target in cancer, Oncology 69 (2005) 11–16.
[27] Y. Takei, K. Kadomatsu, Y. Yuzawa, S. Matsuno, T. Muramatsu, A small interfering RNA targeting vascular endothelial growth factor as cancer therapeutics, Cancer Res. 64 (2004) 3365–3370.
[28] E. Song, P. Zhu, S.K. Lee, D. Chowdhury, S. Kussman, D.M. Dykxhoorn, Y. Feng, D. Palliser, D.B. Weiner, P. Shankar, W.A. Marasco, J. Lieberman, Antibody mediated in vivo delivery of small interfering RNAs via cell-surface receptors, Nat. Biotechnol. 23 (2005) 709–717.
[29] W.J. Kim, L.V. Christensen, S. Jo, J.W. Yockman, J.H. Jeong, Y.H. Kim, S.W. Kim, Cholesteryl oligoarginine delivering vascular endothelial growth factor siRNA effectively inhibits tumor growth in colon adenocarcinoma, Mol. Ther. 14 (2006) 343–350.
[30] H.J. Kim, M. Oba, F. Pittella, T. Nomoto, H. Cabral, Y. Matsumoto, K. Miyata, N. Nishiyama, K. Kataoka, PEG-detachable cationic polyaspartamide derivatives bearing stearoyl moieties for systemic siRNA delivery toward subcutaneous BxPC3 pancreatic tumor, J. Drug Target. 20 (2012) 33–42.
[31] D.M. Euhus, C. Hudd, M.C. LaRegina, F.E. Johnson, Tumor measurement in the nude mouse, J. Surg. Oncol. 31 (1986) 229–234.
[32] A.W. Winkler, H.E. Hoff, P.K. Smith, Cardiovascular effects of potassium, calcium, magnesium, and barium: an experimental study of toxicity and rationale of use in therapeutics, Yale J. Biol. Med. 13 (1940) 123–132.
[33] K. Buyens, M. Meyer, E. Wagner, J. Demeester, S.C.D. Smedt, N.N. Sanders, Monitoring the disassembly of siRNA polyplexes in serum is crucial for predicting their biological efficacy, J. Control. Release 141 (2010) 38–41.
[34] H.J. Kim, A. Ishii, K. Miyata, Y. Lee, S. Wu, M. Oba, N. Nishiyama, K. Kataoka, Introduction of stearoyl moieties into a biocompatible cationic polyaspartamide derivative, PAsp(DET), with endosomal escaping function for enhanced siRNA-mediated gene knockdown, J. Control. Release 145 (2010) 141–148.
[35] H. Takemoto, A. Ishii, K. Miyata, M. Nakanishi, M. Oba, T. Ishii, Y. Yamasaki, N. Nishiyama, K. Kataoka, Polyion complex stability and gene silencing efficiency with a siRNA-grafted polymer delivery system, Biomaterials 31 (2010) 8097–8105.
[36] M.R. Kano, Y. Bae, C. Iwata, Y. Morishita, M. Yashiro, M. Oka, T. Fujii, A. Komuro, K. Kiyono, M. Kaminishi, K. Hirakawa, Y. Ouchi, N. Nishiyama, K. Kataoka, K. Miyazono, Improvement of cancer-targeting therapy, using nanocarriers for intractable solid tumors by inhibition of TGF-β signaling, Proc. Natl. Acad. Sci. U. S. A. 104 (2007) 3460–3465.

Article

pubs.acs.org/Biomac

Dual Environment-Responsive Polyplex Carriers for Enhanced Intracellular Delivery of Plasmid DNA

Mai Sanjoh,[†] Kanjiro Miyata,*[,‡] R. James Christie,[‡] Takehiko Ishii,[§] Yoshinori Maeda,[§] Frederico Pittella,[‡] Shigehiro Hiki,[†] Nobuhiro Nishiyama,[‡] and Kazunori Kataoka*[,†,‡,§,∥]

Departments of [†]Materials Engineering and [§]Bioengineering, Graduate School of Engineering, and [∥]Center for NanoBio Integration, The University of Tokyo, 7-3-1 Hongo, Bunkyo-ku, Tokyo 113-8656, Japan

[‡]Center for Disease Biology and Integrative Medicine, Graduate School of Medicine, The University of Tokyo, 7-3-1 Hongo, Bunkyo-ku, Tokyo 113-0033, Japan

Supporting Information

ABSTRACT: In this study, we describe a multifunctional, nontoxic delivery vehicle with dual-environment sensitivity to deliver plasmid DNA (pDNA) into the cytoplasm of cells. This delivery vehicle was designed to be destabilized by reduction of disulfide cross-links in the intracellular environment and also to contain pH-sensitive membrane-destabilizing activity in acidic late endosomal/lysosomal compartments to allow escape of pDNA into the cell cytoplasm. Polyion complex formation was used to form ternary polyplexes using ionic polymers containing specific chemistries to achieve functional demands. First, template binary polyplexes were formed by association of cationic poly(L-lysine) containing thiol groups (PLys(PDP)) with pDNA and were subsequently cross-linked by disulfide formation for increased stability. Then, binary cross-linked polyplexes were coated with a pH-sensitive membrane-active polyanion, poly(ethylene glycol)-*b*-poly(aspartamide(DET-Aco)) (PEG-PAsp(DET-Aco)), to produce ternary cross-linked polyplexes. PEG-PAsp(DET-Aco) comprises two repeating units of aminoethylene in PAsp side chains and primary amines modified with anionic *cis*-aconitic groups. PEG-PAsp(DET-Aco) degrades at acidic pH to generate the parent PEG-PAsp(DET) polymer, which is active toward late endosomal/lysosomal membranes and thus can assist in the endosomal escape of pDNA following endocytosis. Binary/ternary cross-linked polyplexes remained stable toward counter polyanion exchange with dextran sulfate, but released pDNA following disulfide reduction. Ternary cross-linked polyplexes formed by addition of PEG-PAsp(DET-Aco) resulted in enhanced gene transfection efficiency in cultured cells (Huh-7 and HUVEC) without associated cytotoxicity. The enhanced gene transfection was found to be correlated with improved endosomal escape by observation of intracellular trafficking using confocal laser scanning microscopy. This multifunctional ternary cross-linked polyplex demonstrates the successful design of a gene delivery vehicle utilizing intracellular stimuli, and is a promising platform for further development toward practical use.

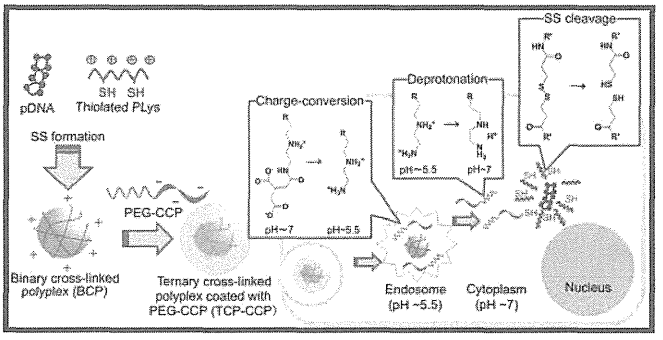

INTRODUCTION

Design of polymeric materials for extra/intracellular delivery of biomacromolecules such as proteins and nucleic acids is currently a major challenge, as slight chemical modifications of those materials can dramatically affect their delivery efficiency. In this regard, polycations have been extensively developed for delivery of plasmid DNA (pDNA),[1−7] as they can electrostatically bind to phosphodiester backbones of nucleic acids to form polyion complexes (termed polyplexes), that protect pDNA from enzymatic degradation and facilitate cellular uptake. To date, a variety of polycations have been reported for polyplex formation that demonstrates enhanced transfection efficiency in vitro and in vivo.[1−7] However, further improvement of polyplex functionality is necessary for enhanced therapeutic efficacy with reduced adverse side effects to allow the translation into practical pharmaceutical agents.

Past efforts have revealed several key functionalities required for successful gene delivery, that is, (i) high stability for pDNA protection, (ii) stealth property for reduced nonspecific interactions with biomacromolecules in the complex extracellular environment in the body, (iii) targetability for delivery into a specific tissue/cell, (iv) endosome-disrupting functionality for translocation into the cytoplasm, (v) efficient release of the pDNA payload into the cytoplasm or the nucleus for efficient transcription, and (vi) low toxicity of the polycation used for polyplex formation. However, several properties demanded for the polyplex carrier are conflicting; high stability versus efficient release of pDNA and biocompatibility versus potentially toxic endosome-disrupting functionality. One of the

Received: July 14, 2012
Revised: September 11, 2012
Published: September 20, 2012

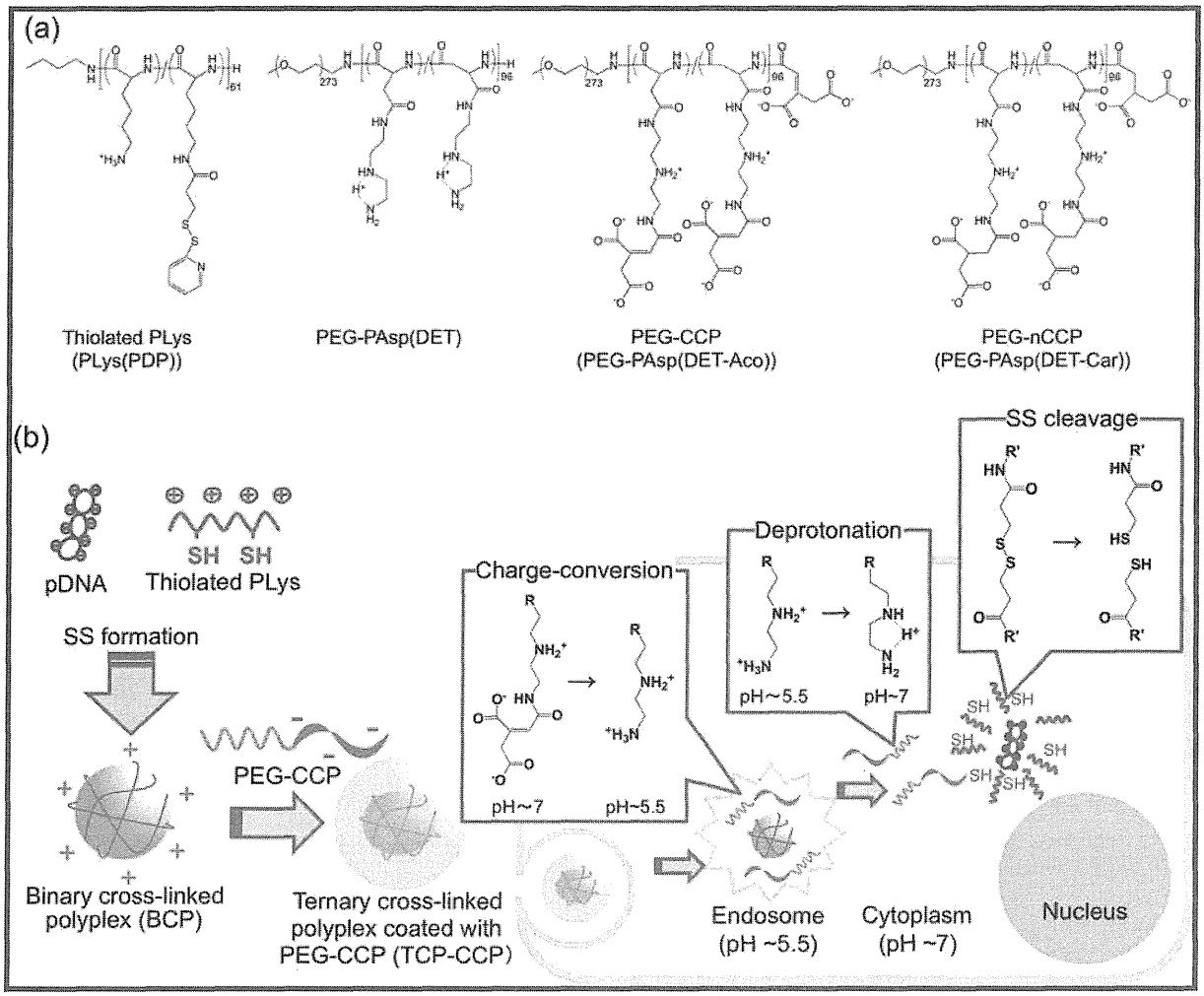

Figure 1. (a) Chemical structures of PLys(PDP), PEG-PAsp(DET), PEG-PAsp(DET-Aco), and PEG-PAsp(DET-Car), with their protonated state at pH 7.4 shown. (b) Schematic illustration for preparation and intracellular trafficking of smart ternary cross-linked polyplexes coated with PEG-CCP (TCP-CCP) with pH and disulfide reduction dual intracellular environment-sensitivity for improved gene delivery.

most promising strategies to overcome these conflicts is to employ "smart" polyplexes that perform a desired function in response to changes in biological microenvironments, for example, the acidic late endosome/lysosome[8] and the reductive cytoplasm/nucleus.[9] Environment-responsive polyplexes have been prepared to exploit these environments by integration of acid-labile imine,[10] hydrazone,[11] acetal,[12] and derivatized maleamate[13−15] linkages or reductive environment-cleavable disulfide bonds[16−24] into the polycation component, aimed toward reversible stability or regulated surface properties (e.g., detachable poly(ethylene glycol) (PEG)-coating) of polyplexes.

For successful gene delivery to be realized, the above-mentioned environment-responsive chemistries must be combined into one multifunctional formulation. For this purpose, coating charged polyplexes with oppositely charged functional polyionic materials (similar to layer-by-layer techniques) is a promising approach due to the ease of manufacturing. Indeed, several previous studies have reported such coated polyplexes, comprising several charged components to impart targetability, endosomal escaping functionality, or biocompatibility.[14,15,25−27] We have previously reported a ternary pDNA polyplex formulated with endosomal membrane-disrupting polyanions to facilitate endosomal escape, which appreciably enhanced gene transfection in cultured cells.[14,15] In this case, the polyanion (abbreviated as PAsp(DET-Aco)) was prepared by modifying a cationic polyaspartamide derivative bearing two repeating units of aminoethylene in each side chain (abbreviated as PAsp(DET)) with *cis*-aconitic anhydride. This modification resulted in anionic groups bound by an acid-labile *cis*-aconitic amide linkage. Polyanionic PAsp(DET-Aco) incorporated into the ternary polyplex degraded in the acidic endosomal environment, thus, regenerating the parent polycation PAsp(DET) for endosome disruption via strong membrane interactions of the diprotonated side chain.[6,28,29] Based on this unique functionality, PAsp(DET-Aco) is termed as a charge-conversional polymer (CCP).[6,14,15,30,31]

The goal of present study was to construct a ternary cross-linked polyplex (TCP) featuring both reversible stability and endosome-disrupting functionality based on dual intracellular environment-sensitivity to disulfide reduction and acidic pH. Thiolated poly(L-lysine) (PLys; Figure 1a) and PEG-PAsp(DET-Aco) (Figure 1a) were prepared and then combined into a ternary polyplex formulation containing disulfide cross-links in the core (Figure 1b). This design is expected to provide the polyplex with high stability and biocompatibility due to disulfide cross-links and a PEG palisade in extracellular media,[16,19,20,23] while regenerating membrane-active PEG-PAsp(DET) in intracellular acidic vesicles to promote endosomal escape (Figure 1b).[14,15] Once in the cytoplasm, the payload pDNA should be released after cleavage of disulfide

bonds in the reductive cytoplasm and nucleus,[16−23] and also deprotonation of PAsp(DET) to the monoprotonated state results in lower cytotoxicity[28,29] (Figure 1b). Formation of TCPs and their dual environment-sensitivity were investigated from a physicochemical standpoint at different pHs and reducing potentials in comparison with a control TCP prepared with a noncharge-conversional polymer (nCCP). Furthermore, biological evaluations in cultured cells were performed to demonstrate the potential of smart TCPs with dual environment-sensitivity for successful gene delivery.

2. EXPERIMENTAL SECTION

2.1. Materials. β-Benzyl-L-aspartate *N*-carboxy anhydride (BLA-NCA) was purchased from Chuo Kaseihin Co., Inc. (Tokyo, Japan). α-Methoxy-ω-amino poly(ethylene glycol) (MeO-PEG-NH_2; M_w = 12000) was obtained from NOF Co, Inc. (Tokyo, Japan). *N*-Methyl-2-pyrrolidone (NMP), diethylenetriamine (DET), dimethyl sulfoxide (DMSO), *N*,*N*-dimethylformamide (DMF), dichloromethane (DCM), and acetic anhydride were purchased from Tokyo Chemical Industry Co. Ltd. (Tokyo, Japan) or Nacalai Tesque (Tokyo, Japan) and used after a conventional distillation. *cis*-Aconitic anhydride and tricarballylic acid were purchased from Sigma-Aldrich Co. (St. Louis, MO). *N*-Succinimidyl 3-(2-pyridyldithio)propionate (SPDP), dithiothreitol (DTT), sodium dextran sulfate (M_w = 5000), and other reagents were purchased from Wako Pure Chemical Industries, Ltd. (Osaka, Japan) and used as received. Ellman's reagent, 5,5-dithiobis-(2-nitrobenzoic acid), and slide-a-lyzer dialysis cassettes (MWCO = 3500 Da) were purchased from Thermo Fisher Scientific Inc. (Waltham, MA). Sterile HEPES (1 M, pH 7.3) was purchased from Amresco (Solon, OH). Spectra/Por dialysis tube (MWCO = 10000 Da) was purchased from Spectrum Laboratories (Rancho Dominguez, CA). The human hepatoma cell line, Huh-7, was purchased from the American Type Culture Collection (Manassas, VA). Dulbecco's Modified Eagle's Medium (DMEM) was purchased from Sigma-Aldrich Co. (St. Louis, MO). Fetal bovine serum (FBS) was purchased from Dainippon Sumitomo Parma Co., Ltd. (Osaka, Japan). Endothelial basal medium-2 (EBM-2) and growth supplements (EGM-2, SingleQuots) were purchased from Lonza (Walkersville, MD). Human umbilical vein endothelial cell (HUVEC) was purchased from Cambrex Corporation (East Rutherford, NJ) and was used within 15 population-doubling times. pDNAs encoding firefly luciferase with a CAG promoter (RIKEN, Tsukuba, Japan) or Gaussia luciferase (GLuc; Nanolight, Pinetop, AZ) were amplified in competent DH5α *E. coli* and purified with a QIAGEN HiSpeed Plasmid MaxiKit (Germantown, MD). Cell Counting Kit-8 and Hoechst 33342 were purchased from Dojindo Laboratories (Kumamoto, Japan). GLuc Assay Kit was purchased from New England Biolabs (Ipswich, MA). Label IT Cy5 Labeling Kit was purchased from Mirus Co. (Madison, WI). LysoTracker Green was purchased from Invitrogen (Molecular Probes, Eugene, OR).

2.2. Synthesis of PLys(PDP): Poly{*N*-[3-(2-pyridyldithio)-propionyl]lysine}. PLys (degree of polymerization (DP): 61; molecular weight distribution (M_w/M_n) = 1.03) was synthesized as previously described.[32] Introduction of 3-(2-pyridyldithio)propionyl (PDP) groups into the primary amines of PLys side chains was performed with a heterobifunctional reagent SPDP. PLys (15.1 mg, 4.37 μmol) and SPDP (3.76 mg, 12.0 μmol) were separately dissolved in 10 mM HEPES buffer (pH 7.4; 3.02 mL) and ethanol (1 mL), respectively. The SPDP solution was added to the PLys solution and stirred at room temperature for 24 h. The polymer product was purified by dialysis against 0.01 N HCl at room temperature for 1 day and then against deionized water at room temperature for 1 day using a dialysis membrane (MWCO = 6000−8000 Da). The dialyzed solution was lyophilized to obtain the final product (14.8 mg, yield 98%) as the chloride salt. The degree of PDP substitution was determined to be 12.2% from the peak intensity ratio of the methyl protons of butylamine (δ = 0.82) to the pyridyl protons of PDP groups (δ = 7.2−8.3 ppm) in ^{1}H NMR spectrum (D_2O, 25 °C; Supporting Information, Figure 1). The NMR analyses in D_2O were performed using 3-(trimethylsilyl)-3,3,2,2-tetradeuteropropionic acid sodium salt (TSPA-d_4) as an internal standard.

2.3. Synthesis of PEG-PAsp(DET-Aco) and PEG-PAsp(DET-Car). *2.3.1. Synthesis of PEG-PAsp(DET): Poly(ethylene glycol)-block-poly{N′-[N-(2-aminoethyl)-2-aminoethyl]aspartamide}.* PEG-PAsp(DET) was prepared as previously reported with a slight modification.[24] Briefly, BLA-NCA (780 mg; 3.13 mmol) was dissolved in DMF (0.7 mL) and then diluted with DCM (7.3 mL). The polymerization of BLA-NCA was initiated from the primary amino group of MeO-PEG-NH_2 (500 mg; 0.0417 mmol) to obtain PEG-PBLA (1100 mg) as a precursor. Size exclusion chromatography (SEC) was performed to determine the molecular weight distribution of the obtained PEG-PBLA using a TOSOH HLC-8220 equipped with TSK gel columns (SuperAW4000 and SuperAW3000 × 2; eluent, NMP with 50 mM LiBr; flow rate, 0.3 mL min^{-1}; temperature, 40 °C) and an internal refractive index (RI) detector. The M_w/M_n was confirmed to be 1.07 from the SEC chart using PEG standards for the calibration (data not shown). The DP of PBLA in PEG-PBLA was determined to be 96 from the peak intensity ratio of the methylene protons of PEG (−OCH_2CH_2−, δ = 3.5 ppm) to the benzyl protons of PBLA ($C_6H_5CH_2$−, δ = 5.1 and 7.3 ppm) in the ^{1}H NMR spectrum (data not shown). Then, lyophilized PEG-PBLA (100 mg, 3.16 μmol) was dissolved in NMP (2.0 mL), followed by the reaction with DET (100 equiv to the benzyl group of PBLA; 3.0 mL, 30.3 mmol) at 0 °C under Ar. The reaction was stopped by dropwise addition of the polymer solution to cold 20% acetic acid (30 mL). The neutralized solution was dialyzed against 0.01 M HCl and then against deionized water at 4 °C. After lyophilization of the dialyzed solution, a white powder was obtained as the chloride salt (91.2 mg, 69.6% yield). The quantitative conversion of the BLA to Asp(DET) was confirmed from the peak intensity ratio of the ethylene protons in PEG (−OCH_2CH_2−, δ = 3.7 ppm) to the ethylene protons in the 1,2-diaminoethane moiety ($H_2N(CH_2)_2NH(CH_2)_2NH$−, δ = 2.8−3.4 ppm) in the ^{1}H NMR spectrum (D_2O, 50 °C; data not shown).

2.3.2. Synthesis of PEG-PAsp(DET-Aco): Poly(ethylene glycol)-block-poly{N″-[N′-(N-cis-aconityl-2-aminoethyl)-2-aminoethyl]-aspartamide}. PEG-PAsp(DET-Aco) was synthesized by the reaction of PEG-PAsp(DET) with *cis*-aconitic anhydride through amide bond formation as previously described.[30,31] Briefly, PEG-PAsp(DET) (17.5 mg, 0.0538 mmol of primary amine) was dissolved in 0.5 M $NaHCO_3$ at pH 9.1 (50 mL). *cis*-Aconitic anhydride powder (420 mg, 2.69 mmol) was added to the solution slowly and stirred at 0 °C for 2 h. The reaction mixture was purified by centrifugal ultrafiltration using an Amicon Ultra filtration device (MWCO = 10000; Millipore (Billerica, MA)), with three centrifugation/rinsing cycles (deionized water) at 4 °C. After lyophilization, the final product was obtained as a white powder (14.9 mg, 64.7% yield). The quantitative conversion of primary amines in Asp(DET) side chain to *cis*-aconitic amide was confirmed from the peak intensity ratio of the methine protons in the main chain (−$COCH_2CH$(CO−)NH−, −$COCH(CH_2$−)NH−, δ = 4.8 ppm) to the methine protons of the *cis*-aconityl moiety (−COC*H*/C(COONa)CH_2COONa, δ = 6.0 ppm) in ^{1}H NMR spectrum (D_2O, 50 °C; data not shown).

2.3.3. Synthesis of PEG-PAsp(DET-Car): Poly(ethylene glycol)-block-poly{N″-[N′-(N-carballylyl-2-aminoethyl)-2-aminoethyl]-aspartamide}. PEG-PAsp(DET-Car) was synthesized using carballylic anhydride as previously described.[30] Briefly, PEG-PAsp(DET) (15 mg, 0.046 mmol of primary amine) was dissolved in 0.5 M $NaHCO_3$ at pH 9.1 (50 mL). Carballylic anhydride powder (363 mg, 2.3 mmol) was added to the solution slowly and stirred at 0 °C for 2 h. The reaction mixture was purified by centrifugal ultrafiltration using an Amicon Ultra filtration device (MWCO = 10000; Millipore (Billerica, MA)), with three centrifugation/rinsing cycles (deionized water) at 4 °C. After lyophilization, the final product was obtained as a white powder (13.5 mg, 68.3% yield). Quantitative conversion of the primary amines in the PAsp(DET) side chain to carballylic amide was confirmed from the peak intensity ratio of the methine protons in the main chain (−$COCH_2CH$(CO−)NH−, −$COCH(CH_2$−)NH−, δ = 4.8 ppm) to the methylene protons of the carballylyl moiety (−CH_2CH(COONa)-

CH_2COONa, δ = 2.5) in the ^1H NMR spectrum (D_2O, 50 °C; data not shown).

2.4. Preparation of Template Binary Cross-Linked Polyplexes (BCPs) and TCPs. PLys(PDP) was dissolved in 10 mM HEPES buffer (pH 7.4) at 5 mg/mL, followed by addition of 50% volume of DTT solution (30.5 mg/mL, 200 mM). The polymer solution was incubated for 30 min at room temperature for cleavage of pyridine 2-thione moiety. Then, the polymer solution was mixed with pDNA solution (50 μg/mL in 10 mM HEPES buffer (pH 7.4)) at a volume ratio of 1:2 (polymer/pDNA) to form BCPs at a residual molar ratio of primary amines in thiolated PLys to phosphates in pDNA = 2. The concentration of pDNA was adjusted to 33 μg/mL in 10 mM HEPES buffer (pH 7.4) and the polyplex solution was further incubated overnight at 4 °C. Then, disulfide cross-linking in the polyplex solution was achieved by oxidation with DMSO. The polyplex solution was dialyzed against 10 mM HEPES buffer (pH 7.4) containing 0.5% v/v DMSO for 36 h (slide-a-lyzer cassette (MWCO = 3500 Da)), followed by 36 h of dialysis against 10 mM HEPES buffer (pH 7.4) for removal of DMSO to yield BCPs. Free thiol content in the polyplex solution was determined by Elman's assay according to the manufacturer's protocol by absorbance measurement at 412 nm and a standard curve generated by reduced glutathione. TCPs were further prepared by addition of PEG-PAsp(DET-Aco) or PEG-PAsp(DET-Car) dissolved in 10 mM HEPES buffer (pH 7.4) to the BCP solution at a residual molar ratio of carboxyl groups in PAsp(DET-Aco) or PAsp(DET-Car) to primary amines in thiolated PLys =1, that is, the residual molar ratio of $[\text{carboxylate}]_{\text{Asp(DET-Aco) or Asp(DET-Car)}}/[\text{secondary amine}]_{\text{Asp(DET-Aco) or Asp(DET-Car)}}/[\text{primary amine}]_{\text{Lys}}/[\text{phosphate}]_{\text{DNA}}$ = 2/1/2/1. The final concentration of pDNA in polyplex solutions was adjusted to 32 μg/mL. Non-cross-linked controls, binary polyplexes (BPs) and ternary polyplexes (TPs), were similarly prepared with nonthiolated PLys.

2.5. Size and ζ-Potential Measurements of Polyplexes. Size measurement was performed at 25 °C using a Zetasizer nanoseries instrument (Malvern Instruments Ltd., U.K.) equipped with a He–Ne laser (633 nm). Each polyplex solution was loaded into a low volume glass cuvette, ZEN2112 (volume: 12 μL; Malvern Instruments, Ltd., U.K.), followed by the measurement. The diffusion coefficient and polydispersity index of polyplexes were determined by the cumulant method, and the corresponding hydrodynamic diameter was calculated using the Stokes–Einstein equation. ζ-Potential of polyplexes was also measured using the same apparatus using a folded capillary cell (Malvern Instruments, Ltd.). The ζ-potential value was calculated by the Smoluchowski equation:

$$\zeta = 4\pi\eta\upsilon/\varepsilon$$

in which ζ is the ζ-potential, η is the viscosity of the solvent, υ is the electrophoretic mobility, and ε is the dielectric constant of the solvent.

2.6. Agarose Gel Electrophoresis. A loading buffer (0.25% bromophenol blue, 0.25% xylene cyanol FF, 30% glycerol in water) was added to each polyplex solution containing 167 ng pDNA. The mixtures were electrophoresed on a 0.9% (w/v) agarose gel with a Tris-acetate running buffer at 100 V for 40 min. The gel was stained with ethidium bromide, and then pDNA bands were visualized under UV illumination using an incident-light fluorescence reader (TAITEC, EU-500M).

2.7. Solution-Based Fluorescence Assay. Each polyplex solution containing 50 ng pDNA was mixed with ethidium bromide (17.3 ng), and the fluorescence intensity of each solution containing ethidium bromide was measured at 590 nm by a fluorospectrometer, NanoDrop ND-3300 (Thermo Fisher Scientific Inc. Waltham, MA). The obtained fluorescence intensity was represented as a percentage of that of naked pDNA mixed with ethidium bromide.

2.8. Transfection Efficiency in Cultured Cells. Transfection efficiency of each polyplex was evaluated by a GLuc assay in cultured Huh-7 cells (or HUVECs). Huh-7 cells (or HUVECs) were seeded at a density of 3000 cells/well in 96-well culture plates and incubated overnight in 100 μL of DMEM (or supplemented EBM-2 for HUVEC) containing 10% FBS. Each polyplex solution containing 0.25 μg pDNA encoding GLuc was added to the cells with fresh medium (n = 5) and further incubated for 48 h. The supernatant of culture media (10 μL) containing GLuc secreted from the cells was mixed with the GLuc assay solution (50 μL). The GLuc activity in the mixture was determined as a photoluminescence intensity (duration time, 2 s; measuring time, 10 s) with a luminometer, Mithras LB 940 (Berthold Technologies, Bad Wildbad, Germany).

2.9. Cytotoxicity. Cytotoxicity of polyplexes was evaluated in cultured Huh-7 cells (or HUVECs). Huh-7 cells (or HUVECs) were seeded in 96-well plates at a density of 3000 cells/well with 100 μL of DMEM (or supplemented EBM-2 for HUVEC) containing 10% FBS, and then incubated for 24 h. Polyplex solution was added to each well (0.25 μg DNA/well; n = 8). After 24 h incubation, the cells were washed with PBS, followed by the addition of fresh DMEM (or supplemented EBM-2 for HUVEC). After 24 h incubation, the cell viability in each well was evaluated using Cell Counting Kit-8 according to the manufacturer's instruction.

2.10. Confocal Laser Scanning Microscopy (CLSM) Observation. pDNA was labeled with Cy5 using a Label IT Nucleic Acid Labeling Kit according to the manufacturer's protocol. Huh-7 cells (5×10^4 cells) were seeded in 35 mm glass base dish (Iwaki, Tokyo, Japan) with 1.2 mL of DMEM containing 10% FBS and incubated for 24 h at 37 °C. Each polyplex solution (90 μL) containing of Cy5-labeled pDNA (2.9 μg) was applied to a dish seeded with cultured Huh-7 cells. After 24 h incubation, the cells were washed three times with PBS. Fresh medium was added to the dish, followed by the incubation for 0, 24, and 48 h without polyplexes. CLSM observation was performed after the staining of the acidic late endosomes/lysosomes with LysoTracker Green and the nuclei with Hoechst 33342. CLSM images were obtained using a LSM 510 microscope (Carl Zeiss, Oberlochen, Germany) with a 63× objective lens at the excitation wavelengths of 488 nm (Ar laser) for LysoTracker Green, 633 nm (He–Ne laser) for Cy5, and 710 nm (MaiTai laser for 2-photon excitation) for Hoechst 33342.

The intracellular distribution of Cy5-labeled pDNA was quantitatively evaluated by calculating the colocalization ratio of Cy5-labeled pDNA pixels with LysoTracker Green pixels. The calculation was conducted as follows:

$$\text{colocalization ratio} = \text{yellow pixels(colocalization of Cy5 with LysoTracker Green)} / \text{yellow and red pixels(all the Cy5 in cells)}$$

The results are expressed as mean and standard error of mean (SEM) obtained from 20 cells.

2.11. Data Analysis. The experimental data was analyzed by Student's t-test. $P < 0.05$ was considered as statistically significant.

3. RESULTS AND DISCUSSION

3.1. Synthesis of Thiolated PLys (PLys(PDP)), PEG-CCP (PEG-PAsp(DET-Aco)), and PEG-nCCP (PEG-PAsp(DET-Car)). SPDP was reacted with PLys (DP = 61) to introduce protected thiol groups into the side chain of PLys via an amide linkage. The degree of thiolation was targeted to be approximately 10%, as our previous studies showed that PEG-PLys with 11% thiolation formed PEGylated cross-linked polyplexes that exhibited long-lasting gene expression in cultured cells as well as significant gene expression in a subcutaneous tumor tissue via systemic administration.[33,34] The obtained degree of thiolation was determined to be 12.2% as calculated from the peak intensity ratio of the methyl protons of butylamine ($CH_3CH_2CH_2CH_2NH-$, δ = 0.82) to the pyridyl protons of the PDP groups (C_5H_4N, δ = 7.20–8.30 ppm) in ^1H NMR spectrum (Supporting Information, Figure 1).

PEG-PAsp(DET), the precursor of PEG-PAsp(DET-Aco), was prepared by the aminolysis reaction of PEG-PBLA with

DET. The DP of Asp(DET) units in the obtained polymer was calculated to be 96 from ^{1}H NMR spectrum and a narrow molecular weight distribution (M_w/M_n = 1.07) was confirmed by SEC analysis. PEG-PAsp(DET-Aco) was synthesized by the reaction of *cis*-aconitic anhydride with primary amines in the PAsp(DET) side chains (Figure 1a). The quantitative conversion to *cis*-aconitic amide was confirmed from the peak intensity ratio of the methine protons in the main chain ($-COCH_2CH(CO-)NH-$, $-COCH(CH_2-)NH-$, δ = 4.8 ppm) to the methine protons of the *cis*-acontityl moiety ($-COCH/C(COONa)CH_2COONa$, δ = 6.0 ppm) in the ^{1}H NMR spectrum (data not shown). Asp(DET-Aco) units were considered to have a net charge of −1 at pH 7.4 because they contain two deprotonated carboxylates and one protonated secondary amine. The *cis*-aconitic moiety in Asp(DET-Aco) units rapidly degrades at endosomal pH ~5.5 to regenerate Asp(DET) units (Figure 1b).[14,15] The regenerated PAsp(DET) segment featuring the diprotonated state can then facilitate the endosomal escape of polyplexes by endosomal membrane disruption. A control polymer lacking pH-sensitivity, PEG-PAsp(DET-Car), was synthesized in a similar fashion by modification of PAsp(DET) with carballylic anhydride (Figure 1a). PEG-PAsp(DET-Car) has two carboxylates and one secondary amine, similar to PEG-PAsp(DET-Aco), but contains a nonacid-labile carballylic amide. Quantitative conversion of primary amines in Asp(DET) side chain to carballylic amides was also confirmed from the ^{1}H NMR spectrum (data not shown).

3.2. Preparation of BCPs and TCPs. Thiolated PLys was first reduced with DTT to generate free thiols and then mixed with pDNA at the molar ratio of primary amine to phosphate = 2 to form template BCPs. Polyplex formation with thiolated PLys was successful at this mixing ratio, as free pDNA was not observed in an agarose gel electrophoretic analysis (data not shown), indicating that all of the pDNAs were effectively encapsulated. The prepared polyplexes were then cross-linked through disulfide bond formation in the presence of an oxidizing reagent (DMSO) after removal of DTT. The BCPs obtained were subjected to Ellman's test for estimation of residual thiol groups and cross-linking efficiency. Disulfide cross-linking was found to be very efficient, as thiolated PLys contained 0.1 mM thiol groups before cross-linking (at the same concentration as the polyplex solution), whereas oxidized BCP solution contained only 0.002 mM free thiol. Thus, 98% of thiol groups in BCPs were converted to disulfide bonds. Next, the size and ζ-potential of BCPs were evaluated by dynamic light scattering (DLS) and laser Doppler electrophoresis, respectively. BCPs were found to have a hydrodynamic diameter of 82 nm with narrow size distribution (polydispersity index (PDI) = 0.10) and a substantially positive ζ-potential of +25 mV (Table 1 and Supporting Information, Figure 2). For comparison, binary non-cross-linked polyplexes prepared from nonthiolated PLys (BPs) exhibited a hydrodynamic diameter of 76 nm and PDI = 0.12, indicating no remarkable size difference between cross-linked and non-cross-linked polyplexes.

Table 1. Size, Polydispersity Index (PDI), and ζ-Potential of Polyplexes at pH 7.4

sample	hydrodynamic diameter (nm)	PDI	ζ-potential (mV)
BP	76	0.12	+25
BCP	82	0.10	+25
TCP-CCP	89	0.07	+2

TCPs were prepared by electrostatically coating the cationic BCPs with anionic PEG-CCP (or PEG-nCCP as a control) to generate TCP-CCPs (or TCP-nCCPs). The mixing composition was set at the residual molar ratio of carboxylates in PAsp(DET-Aco) to primary amines in thiolated PLys =1. This mixing ratio corresponds to a charge stoichiometric point among PEG-CCP, thiolated PLys, and pDNA, that is, $[COO^-]_{Asp(DET\text{-}Aco) \text{ or } Asp(DET\text{-}Car)}/[NH_2^+]_{Asp(DET\text{-}Aco) \text{ or } Asp(DET\text{-}Car)}/[NH_3^+]_{Lys}/[PO_4^-]_{DNA}$ = 2/1/2/1, presumably minimizing the amount of free polymers in the polyplex solution. This charge-neutral formulation was chosen for less toxic gene delivery, considering the fact that polyplexes comprised of polyethyleneimine and its derivatives induce significant cytotoxicity due to an excess of free polymer in solution.[35,36] To confirm the formation of TCPs, size and ζ-potential measurements were performed. TCP-CCPs exhibited a hydrodynamic size of 89 nm and PDI of 0.07, indicating slightly larger size and similar PDI compared to the template BCPs (Table 1 and Supporting Information, Figure 2). The ζ-potential of BCPs decreased from +25 to +2 mV by coating with PEG-CCP, which is in sharp contrast with the ζ-potential of the previously reported ternary polyplexes formed with non-PEGylated CCP (<−20 mV).[14,15] Both the increased size and the almost neutral ζ-potential of the TCPs indicate successful coating of BCPs with a nonionic, biocompatible PEG palisade. Note that a free pDNA band was not detected in agarose gel electrophoretic analysis of TCP-CCPs, indicating that no pDNA release was associated with the polyanion-coating process (Figure 3a).

3.3. pH-Sensitivity of TCPs. The TCP-CCP formulation was desired to be stable at extracellular/cytoplasmic neutral pHs, but degradable at the acidic pH of late endosomal/lysosomal subcellular compartments due to degradation of *cis*-aconitic amides in PAsp(DET-Aco) segment to regenerate the parent PEG-PAsp(DET) polymer (Figure 1b). Thus, the acidic pH-sensitivity of TCPs was investigated by ζ-potential measurement (Figure 2). This experiment allows to monitor degradation of *cis*-aconitic moieties because the polyplex surface charge is expected to increase with loss of *cis*-aconitic moieties in PAsp(DET-Aco) segment.[14,15] As shown in Figure 2a, TCP-CCPs maintained the initial ζ-potential (+2 mV) for 18 h at pH 7.4. At pH 5.5, however, the ζ-potential gradually increased to +20 mV (comparable to the ζ-potential of BCPs (Table 1)) over 18 h. This result indicates that the cationic surface of the template BCPs was exposed by detachment of PEG-PAsp(DET/DET-Aco) from the TCP-CCPs (due to charge repulsion) in the acidic environment. To confirm the necessity of the *cis*-aconitic amide bond for acidic pH-sensitivity, the experiment was also performed with the control lacking charge-conversion functionality. Control TCP-nCCPs maintained the initial ζ-potential (+2 mV) at both pH 7.4 and 5.5 for 18 h (Figure 2b). These results confirmed that TCP-CCPs exhibited the desired endosomal acidic pH-sensitivity due to *cis*-aconitic moieties.

3.4. Reductive Environment-Sensitivity of BCPs and TCP-CCPs. Disulfide cross-links were incorporated into the template BCPs to impart reversible stability in response to the reducing potential of the intracellular environment.[9] Polyplex stability was investigated by counter polyanion exchange with dextran sulfate in both nonreductive and reductive conditions. On the agarose gel electrophoretic analysis, released pDNA

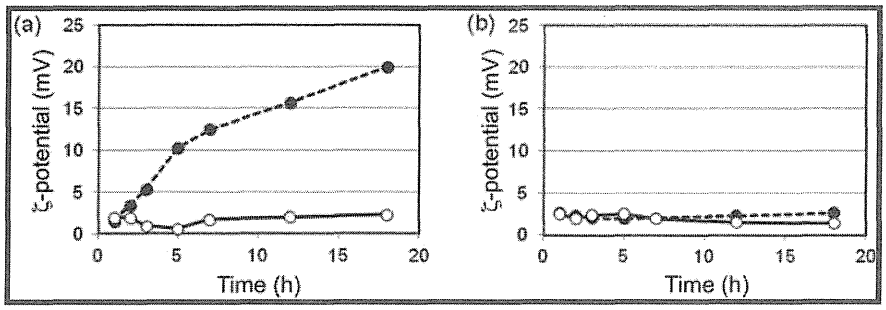

Figure 2. Time-dependent change in the ζ-potential of (a) TCP-CCPs and (b) TCP-nCCPs at pH 7.4 (open circle) and 5.5 (closed circle).

bands were clearly observed for both non-cross-linked BPs and their ternary polyplexes with PEG-CCP (TP-CCPs) after overnight incubation with dextran sulfate under a nonreductive condition, indicating polyplex dissociation (Figure 3a). In contrast, the naked pDNA band was not observed for both BCPs and TCP-CCPs in the same conditions (Figure 3a), indicating that the disulfide cross-links substantially stabilized the polyplex against counter polyanion exchange under nonreductive conditions. Next, the pDNA release behavior of BCPs and TCP-CCPs was similarly investigated under reductive conditions in the presence of DTT. Although the pDNA release from cross-linked polyplexes (BCPs and TCP-CCPs) was not apparently completed in comparison with naked pDNA, the bands of released pDNA were clearly observed for both cross-linked formulations, similar to non-cross-linked controls (BPs and TP-CCPs), after addition of dextran sulfate, indicating dissociation of BCPs and TCP-CCPs due to the cleavage of disulfide cross-links under reductive conditions. In addition, the reductive environment-sensitivity of BCPs and TCP-CCPs was more quantitatively compared to control BPs and TP-CCPs in an ethidium bromide exclusion assay (Figure 3b). In the nonreductive condition, addition of dextran sulfate drastically increased the fluorescence intensity of BPs and TP-CCPs at a comparable level to naked pDNA, indicating significant decondensation of pDNA allowing the intercalation of ethidium bromide. In contrast, BCPs and TCP-CCPs did not exhibit significant increase in the fluorescence intensity in the nonreductive condition, while showing the comparable fluorescence intensity to BPs and TP-CCPs in the reductive condition, suggesting substantial destabilization of the cross-linked polyplexes. These results demonstrate the reversible stability of both BCPs and TCP-CCPs in response to disulfide reduction.

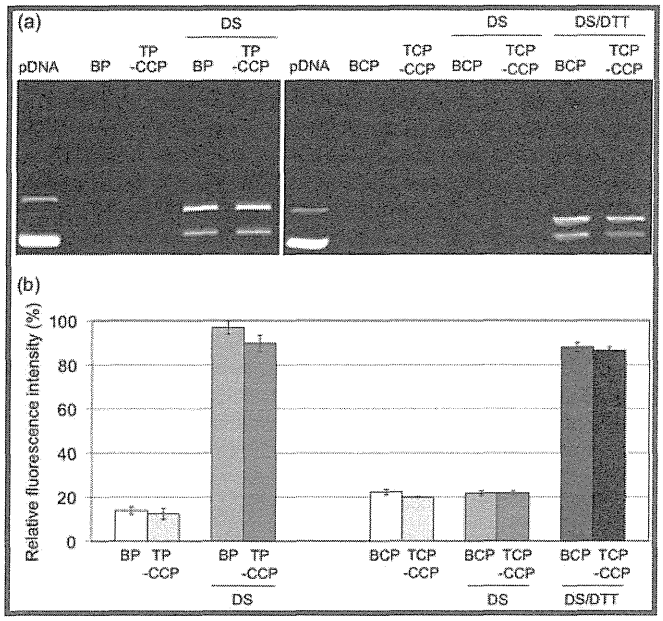

Figure 3. (a) Agarose gel electrophoretic analysis of BPs, TP-CCP, BCPs, and TCP-CCPs in the absence/presence of DS and DTT. (b) Ethidium bromide exclusion assay of BPs, TP-CCPs, BCPs, and TCP-CCPs in the absence/presence of DS and DTT. The fluorescence intensity was represented as a percentage of that of naked pDNA mixed with ethidium bromide. Results are expressed as mean and SD (n = 3). DS, dextran sulfate (sulfate/phosphate = 20:1), and DTT, 25 mM dithiothreitol.

3.5. In Vitro Gene Expression. The ability of polyplexes to transfect cells with a target gene was assessed using polyplexes loaded with pDNA encoding the bioluminescent enzyme GLuc. Successful transfection of GLuc gene results in the secretion of GLuc proteins from transfected cells into the cell culture medium. Thus, addition of GLuc substrate luciferin to the cell culture supernatant results in the emission of light which can be

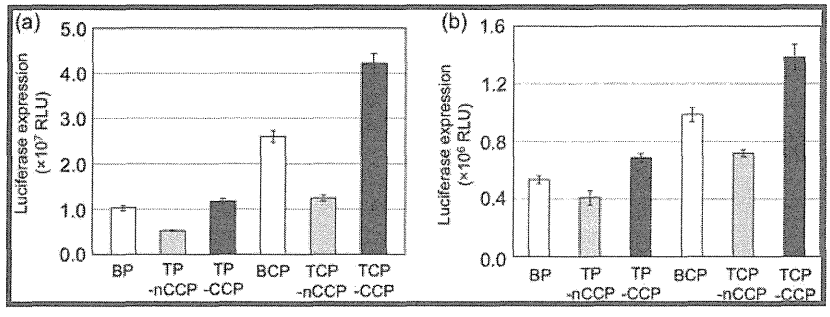

Figure 4. Transfection efficiency of polyplex formulations in cultured (a) Huh-7 cells and (b) HUVECs. Cells were incubated with each polyplex for 48 h prior to analysis. Results are expressed as mean and SEM (n = 5).

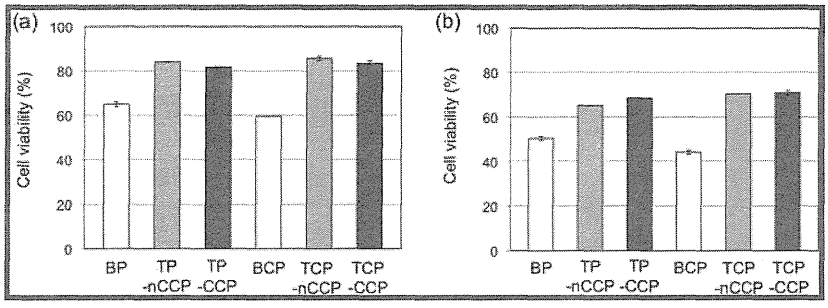

Figure 5. Cell viability of (a) Huh-7 cells and (b) HUVECs treated with polyplex formulations at the same conditions as the transfection assay shown in Figure 4. Results are expressed as mean and SEM (n = 8).

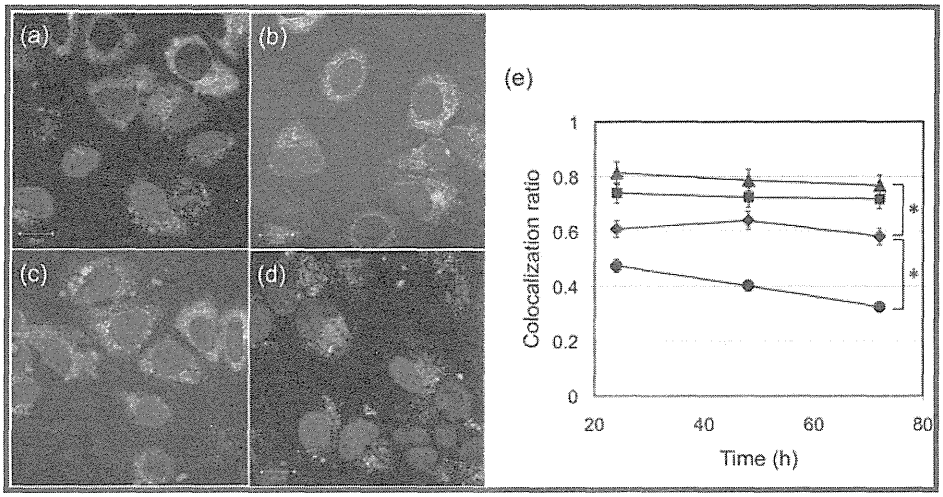

Figure 6. Intracellular distribution of Cy5-labled pDNA delivered by (a) BPs, (b) BCPs, (c) TCP-nCCPs, and (d) TCP-CCPs in Huh-7 cells after 48 h incubation. (e) Colocalization ratio of Cy5-labled pDNA with the late endosome/lysosome stained by LysoTracker Green. BPs (closed square), BCPs (closed diamond), TCP-nCCPs (closed triangle), and TCP-CCPs (closed circle). Results are expressed as mean and SEM from 20 cells. *P < 0.01 compared to BCP at all the tested time points.

measured using a photon counter. This assay was performed in both Huh-7 cells and HUVECs to determine whether the in vitro transfection profile of TCPs depends on cell type (Figure 4a,b). Obviously, disulfide cross-linked formulations (BCPs, TCP-nCCPs, and TCP-CCPs) showed higher transfection efficiency compared to the corresponding non-cross-linked controls (BPs, TP-nCCPs, and TP-CCPs, respectively) in both cell types, indicating that disulfide cross-linking enhanced polyplex transfection efficiency, regardless of the coating with PEG-CCP/PEG-nCCP, probably due to the stabilization effect in cell culture medium as well as in the endosome/lysosome.[23,33] Coating BCPs with PEG-CCP to generate TCP-CCPs further enhanced the transfection efficiency for both cell types, whereas coating BCPs with PEG-nCCP decreased the transfection efficiency. These results demonstrate that PEG-CCP improved the polyplex transfection efficiency based on the charge-conversional property. It should be noted that the reduced transfection efficiency of TCP-nCCPs, compared to the template BCPs, might be due to the compromised endosomal escape of polyplexes due to the acidic pH-insensitive, stable PEG palisades (PEG dilemma).[24] This issue will be further examined in the next section. The obtained transfection profiles were similar between Huh-7 cells and HUVECs, suggesting that the effect of PEG-CCP and disulfide cross-linking on enhanced trasnfection might not be limited to a specific cell type.

In addition to higher transfection efficiency, lower cytotoxicity is also necessary for successful gene therapy. Thus, the cytotoxicity of TCPs was investigated under conditions similar to the GLuc transfection assay described above. As shown in Figure 5a,b, the viability of cells treated with ternary formulations (TPs and TCPs) was obviously higher than that treated with binary formulations (BPs and BCPs) in both cell types. Thus, coating BPs/BCPs with PEGylated polyanions (PEG-CCP and PEG-nCCP) substantially reduced the cytotoxicity of the template polyplexes, probably due to the reduced nonspecific interactions of positively charged polyplexes with the oppositely charged cytoplasmic membrane. In this regard, the PEG palisade in TPs and TCPs was found not to affect the cytotoxicity, as non-PEGylated ternary controls[15] induced the similar cytotoxicity profile in the tested transfection condition (data not shown), suggesting that the coating with polyanions might be crucial for lower cytotoxicity in ternary formulations. Nevertheless, the PEG palisade in TPs and TCPs is expected to play an essential role for reduced nonspecific interactions with biological components in harsh in vivo situation.[37] Meanwhile, the similar cytotoxicity between TCP-CCPs and TCP-nCCPs indicates that PEG-CCP does not induce additional cytotoxicity associated with the charge-conversion and regeneration of the PAsp(DET) polycation after migrating into the cell interior. This apparent lack of additional cytotoxicity of PEG-CCPs (or PEG-PAsp(DET) generated in the acidic vesicles) can be explained by the fact that the side chains of PAsp(DET) adopt an appreciably less toxic monoprotonated structure in the neutral cytoplasm (Figure 1b).[28,29] The transfection efficiency and cytotoxicity